

Toppling susceptibility of a single rock block resting on a regularly rough base

Jing-Yun Gui^{a,b}, Manuel A. González-Fernández^b, Xian Estévez-Ventosa^b, Fei Song^c, Leandro R. Alejano^{b,*}

^a College of Geological Engineering & Surveying and Mapping, Chang'an University, Xi'an, Shaanxi, PR China

^b GESSMin Group, CINTECX, Department of Natural Resources and Environmental Eng, University of Vigo, Spain

^c Department of Civil and Environmental Engineering, Universitat Politècnica de Catalunya (UPC), Barcelona 08034, Spain

ARTICLE INFO

Keywords:

Rock slope
Toppling
Stability
Rough base
Discrete element modelling
Analytical solution

ABSTRACT

Toppling of individual rock blocks resting on an inclined surface has often been observed in nature. This instability mechanism has typically been analysed for simple block geometries, considering the contact between the block and the base where it lies is a planar surface. In this study, the authors analyse the case where this contact is a regularly rough surface. To do that, the authors resort to analytical limit equilibrium formulations, laboratory physical models and discrete element methods. All these approaches show a consistent trend of behaviour, where roughness does affect the toppling response. Regularly rough surfaces are studied in detail and a general analytical formulation able to show the potential influence of roughness on the block toppling response is derived. Additionally, some considerations are provided regarding the combined effects of rough bases and rounded corners on toppling stability. The authors show how under particular circumstances, roughness can control the potential failure mechanism of a block to produce toppling instead of sliding, and they eventually discuss the impact of rough bases on the toppling response of natural rock blocks.

1. Introduction

A key issue for rock slope stability analysis is the identification of the potential failure mechanism of individual elements. Once it is identified, the stability of the slope can be analysed based on the rigorous estimate of the geometry of the potential failure and the geomechanical parameters of the discontinuities and materials at stake (Hoek and Bray, 1974; Stead and Wolters, 2015).

Traditional rock slope stability approaches typically contemplate planar, wedge, circular, and toppling failure as potential instability mechanisms. Whereas planar or wedge failure involve a small number of discontinuities, toppling phenomena involve many more. This renders the analysis more complex and less reliable. Moreover, toppling failure can generate different types of mechanisms involving one or various blocks (Wyllie and Mah, 2004).

Additionally, the potentially rotating blocks can be fully detached from the rock mass due to pre-existing discontinuities or only partially detached, in which case the mechanism will involve flexural toppling (Aydan and Kawamoto, 1992; Adhikary et al., 1996; Adhikary and

Dyskin, 2007), which needs to overcome tensile strength of part of a block. Analysis of single-block toppling cases were considered by early researchers (Ashby, 1971; Hoek and Bray, 1974; Sagaseta, 1986) assuming regular slab-like shaped and sharp-cornered blocks resting on planar tilted surfaces. These simple analyses were later on incorporated into more complex, multiple-element toppling models (Goodman and Bray, 1976). The last author of this paper has recently extended these studies to the case of more irregular blocks (Alejano, 2021).

Some authors (Martin, 1990; Sjöberg, 1999) have suggested that failures associated with large-scale or deep-seated toppling are among the most common and relevant failure mechanisms in large rock open pit slopes. Nevertheless, these complex phenomena seem to be still not well understood (Muralha, 2002; Brideau and Stead, 2010). These toppling-related mechanisms are rather common according to the authors' experience and literature surveys (Alejano et al., 2010; Böhme et al., 2013; Gu and Huang, 2016; Amini et al., 2017; Amini and Ardestani, 2019; Alejano et al., 2019; Pérez-Rey et al., 2019) and still poorly known.

Therefore, this study focuses on analysing the stability of a single

* Corresponding author.

E-mail address: alejano@uvigo.es (L.R. Alejano).

block resting on a regularly rough surface which may have a relevant impact on single-block toppling failure, affecting also the stability of more complex toppling related instabilities.

Block stability against toppling can be analysed based on analytical techniques (Ashby, 1971; Goodman and Bray, 1976), numerical methods (Ishida, 1990; Barla et al., 1995; Lanaro et al., 1997) and physical models (Pérez-Rey et al., 2021). A combination of these approaches is recommended with the aim of better understanding the mechanisms at stake and the relevance of the different parameters to stability. In this study, these techniques will be briefly recalled and resorted to.

2. Previous studies

2.1. Failure mechanisms involving toppling

Toppling involves the rotation of rock columns or blocks about a fixed axis. This mechanism may include one single block or various blocks (Fig. 1). Additionally, two different mechanical toppling mechanisms may take place. If the block or blocks prone to topple are already detached from the rock mass, the mechanism will be standard toppling. If not, we will refer to flexural toppling. Figs. 1a, c and d illustrate standard toppling scenarios, where blocks are fully detached from the rest of the rock mass. Figs. 1b, e and f show cases where blocks are not fully detached from the rock mass, so failure will involve flexural toppling.

The simplest toppling mechanisms involve a single block. The stability analysis of such cases is relatively simple (Ashby, 1971; Hoek and Bray, 1974; Sagaseta, 1986). Fig. 1a to c illustrates these mechanisms. If the block is not detached, a flexural toppling mechanism is prone to occur, so computations need to consider the role of rock tensile strength.

However, the most common toppling failures found in nature involve several blocks. According to Goodman and Bray (1976), block toppling, flexural toppling, and block flexural toppling are the most frequent toppling failures of this kind involving some or many blocks. Wyllie and Mah (2004) described these mechanisms, illustrated in Fig. 1d to f, in more detail.

Goodman and Bray (1976) and Wyllie and Mah (2004) among others have suggested the possible occurrence of a number of secondary toppling mechanisms. This refers to other mechanisms where toppling, as a behaviour mode, is excited by any other independent phenomenon where toppling would be otherwise unlikely to occur. A typical example

would be a mechanism initiated by undercutting of the toe of the slope, which induces toppling in the crest of the slope. Also, complex failure mechanisms involving partial toppling combined with other sliding mechanisms have been described and analysed in the literature (Stead et al., 2006; Alejano et al., 2010, 2019; Gu and Huang, 2016; Amini et al., 2017). Secondary toppling and toppling combined with other mechanisms fall out of the scope of this study.

The stability analysis against toppling was traditionally addressed based on analytical limit equilibrium methods (LEM) resorting to moment equilibrium equations. In early studies on toppling, simple physical models were also performed to check analytical approaches (Ashby, 1971), later extended to a wider number of situations and blocks of more complex geometry (Zhang et al., 2007; Alejano et al., 2015, 2018a; Pérez-Rey et al., 2019, 2021). Moreover, from the early developments of numerical modelling, discrete element approaches have been applied to analyse toppling phenomena (St John, 1972; Adhikary and Dyskin, 2007; Zheng et al., 2019). In the current study, all these three methods have been used together to analyse the problem at stake. Analytical, physical, and numerical approaches in the context of this study are briefly introduced in the following sub-sections.

Even if single block toppling (Fig. 1a) has been rigorously studied for different geometries (Alejano et al., 2015; Pérez-Rey et al., 2019), no studies have addressed in due detail the case where the base of the block is a rough surface (Fig. 1c). In this paper, the authors present a first study analysing this contingency for the case of regularly rough bases. It will also be relevant to study how irregularly or unevenly rough bases affect single block toppling and how rough bases will affect block toppling of many blocks, but these topics fall out of the scope of this study.

2.2. Analytical approaches

The analytical approach to compute the stability of a block against toppling relies on the limit equilibrium method (LEM). The approach is generally set out in the form of a factor of safety formulation according to Eq. (1), which relates the stabilizing and overturning moments of all the forces acting in the block in relation to the position of the potential overturning axis, which needs to be previously identified.

$$FoS_{toppling} = \frac{\sum M_{stabilising}}{\sum M_{overturning}} \quad (1)$$

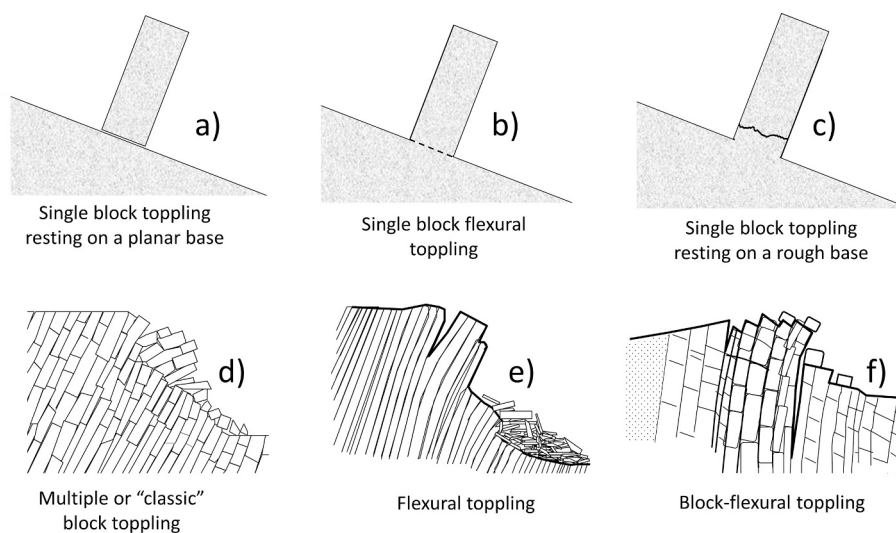


Fig. 1. Different mechanisms of single block toppling (upper row) and multiple block toppling (lower row): a) Toppling of a single-detached regular block b) Flexural toppling of a single block c) Toppling of a single-detached block with a rough base d) Block toppling of many blocks e) Flexural toppling of many blocks or slabs and f) Block-flexural toppling.

2.2.1. Stability of regular blocks

For a regular slab-like block resting on a tilted plane (Fig. 2a), the stability can be computed according to Eq. (2), as proposed by Ashby (1971) and other researchers (Hoek and Bray, 1974; Goodman and Bray, 1976):

$$FoS = \frac{M_{stabilizing}}{M_{overturning}} = \frac{\frac{\Delta x}{2} \cdot W \cdot \cos \alpha \cdot z}{\frac{y}{2} \cdot W \cdot \sin \alpha} = \tan^{-1} \alpha \cdot \left(\frac{\Delta x}{y} \right) \quad (2)$$

$\Delta x/y$ is the inverse of slenderness. Based on this equation, a graph of potential instability mechanisms of a block can be plotted to analyse its trend towards sliding or toppling (Sagaseta, 1986). Additionally, by setting $FoS = 1$, one can derive the critical toppling angle, provided it is larger than the critical friction angle of the contact (otherwise the block will slide):

$$\alpha_{crit.} = \tan^{-1} \left(\frac{\Delta x}{y} \right) \quad (3)$$

2.2.2. Stability of blocks with rounded corners

When observing fallen blocks with eroded corners in the field, Alejano et al. (2015) realized that, for rock slabs or blocks presenting regular rounded corners, the potential rotation axis moves against dip. So, the trend to topple of round-cornered (of radius r) block (Fig. 2b) is larger than that of an equal size, sharp-cornered block, and it can be rigorously computed according to Eq. (4):

$$FoS = \frac{M_{stabilizing}}{M_{overturning}} = \frac{\left(\frac{\Delta x}{2} - r \right) \cdot W \cdot \cos \alpha \cdot z}{\frac{y}{2} \cdot W \cdot \sin \alpha} = \tan^{-1} \alpha \cdot \left(\frac{\Delta x - 2r}{y} \right) \quad (4)$$

This is relevant to this study because when cutting small blocks in the lab, it is difficult to obtain perfectly sharp-cornered blocks, and the irregularities of the corner can be analysed with the help of an equivalent radius of curvature (r_c) of the corner at stake. Note that the tilt angle at which the round-cornered block topples, also called critical angle, can be derived from Eq. (5).

$$\alpha_{crit.} = \tan^{-1} \left(\frac{\Delta x - 2r}{y} \right) \quad (5)$$

2.3. Physical modelling

Physical modelling of blocks for studying toppling implies preparation of blocks with homothetic geometries to those under study. Similarity laws are fulfilled if homogeneous blocks (all material density equal) are used. These blocks are initially positioned on a horizontal

base platform, which is then progressively tilted until sliding or toppling is observed. The toppling or sliding angle can be then compared with that determined from other approaches (analytical, numerical, etc.). Tests are typically repeated three times and the average value is computed as the relevant result. According to authors' experience, toppling critical angles tend to be rather uniform. However, sliding critical angles usually show higher variability due to the more complex nature of frictional sliding.

Any block with the same geometry independently of its size will theoretically topple at the same critical angle. Only imperfections on the block corners and edges may slightly influence results. In conclusion, the application of physical modelling has been sufficiently verified for studying the toppling (and sliding) mechanism in rock blocks (Alejano et al., 2015; Pérez-Rey et al., 2019, 2021).

For this study, relatively small block specimens with a regularly rough contact base were prepared. The tilt tests were performed with a tilting table designed by the University of Vigo (Fig. 3) (Alejano et al., 2018b), where the block was placed on a horizontal platform and then the platform was tilted at a constant velocity until an instability phenomenon was observed.

Physical toppling models for more complex geometries including flexural toppling typically resort to centrifuge tests that can produce failure in these more stable structures (Adhikary and Dyskin, 2007; Zhang et al., 2007).

2.4. Numerical approaches: DEM modelling

Numerical models can also be used to analyse toppling failure mechanisms and they are well suited to work with complex block geometries. The Distinct Element Method (DEM), first proposed by Cundall (1971), associated with explicit integration approaches, is able to simulate both rigid and deformable blocks to model large displacements and rotations of block systems.

In this research, the DEM-based universal distinct element code (UDEC) (ITASCA Cons. Group Inc, 2014) was selected to simulate the instability mechanism of blocks against toppling or sliding. UDEC has been widely used to study block systems in civil engineering and mining for decades (Alejano et al., 2012). It can include considerations of some dynamic and coupled processes that are difficult to address using standard approaches (Mendes et al., 2020). Additionally, even when there exist various blocks and tensile failure appear, still a factor of safety can be computed based on strength reduction techniques (Dawson et al., 1999; Alejano and Alonso, 2005).

In the numerical simulations herein, the models are built with a

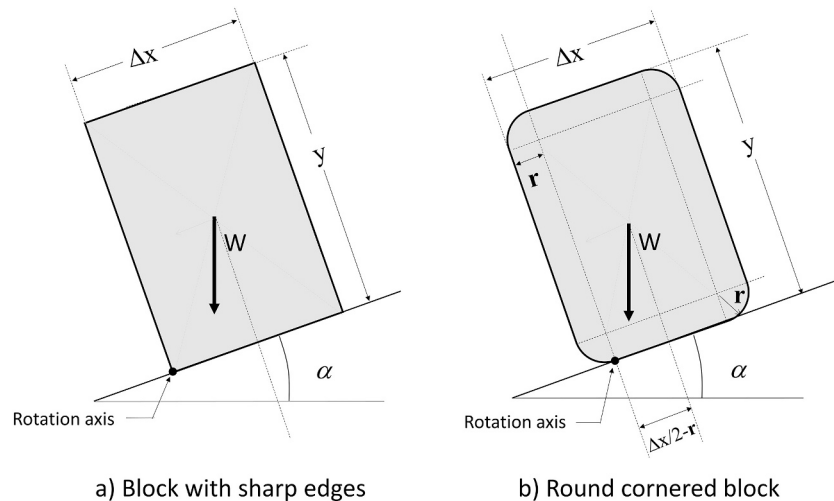


Fig. 2. Representation of a) standard (sharp-cornered) Δx -width and y -height block resting on a tilted surface and b) round-cornered block of equal dimensions with corner radius r .



Fig. 3. Tilting system used for the physical models developed at the University of Vigo.

predetermined geometry. The block is located on a platform with the lower regular base fixed. Tentative models with various inclination angles are tested to bracket the critical angle at which the block topples or slides, as shown in Fig. 4.

The stability against toppling of more complex elements can be studied by 3DEC (ITASCA Cons. Group Inc, 2019) numerical simulations. For these numerical studies, geomechanical parameters such as the normal and shear stiffness in the contact plane should be selected with care according to estimative techniques (Brideau and Stead, 2010; Muñiz-Menéndez et al., 2020). Additionally, based on this approach, static, pseudo-dynamic, and dynamic calculations can be performed (Lemos et al., 2011).

3. Preparation of samples and geometries

3.1. Experimental program

Based on the approaches introduced in the previous section, the authors decided to carry out an experimental program to test against toppling small rock samples presenting a regularly rough base formed by triangular teeth of known dimensions. To do that, it was decided to create 7 blocks with various slenderness able to produce toppling or sliding, and regularly rough surfaces following the geometrical parameters illustrated in Fig. 5. The rock used was a hard granite with a specific weight of 25.8 kN/m³ and a uniaxial compressive strength about 120 MPa; the used glue was a standard cyanoacrylate adhesive.

These blocks were created using 2, 3 or 4 narrow slender rectangular rock slabs that were bevelled at a particular height with an angle of roughly 10° or 20°. Then, these individual blocks were assembled by gluing the sides with same height to create the final symmetric (for 2 and

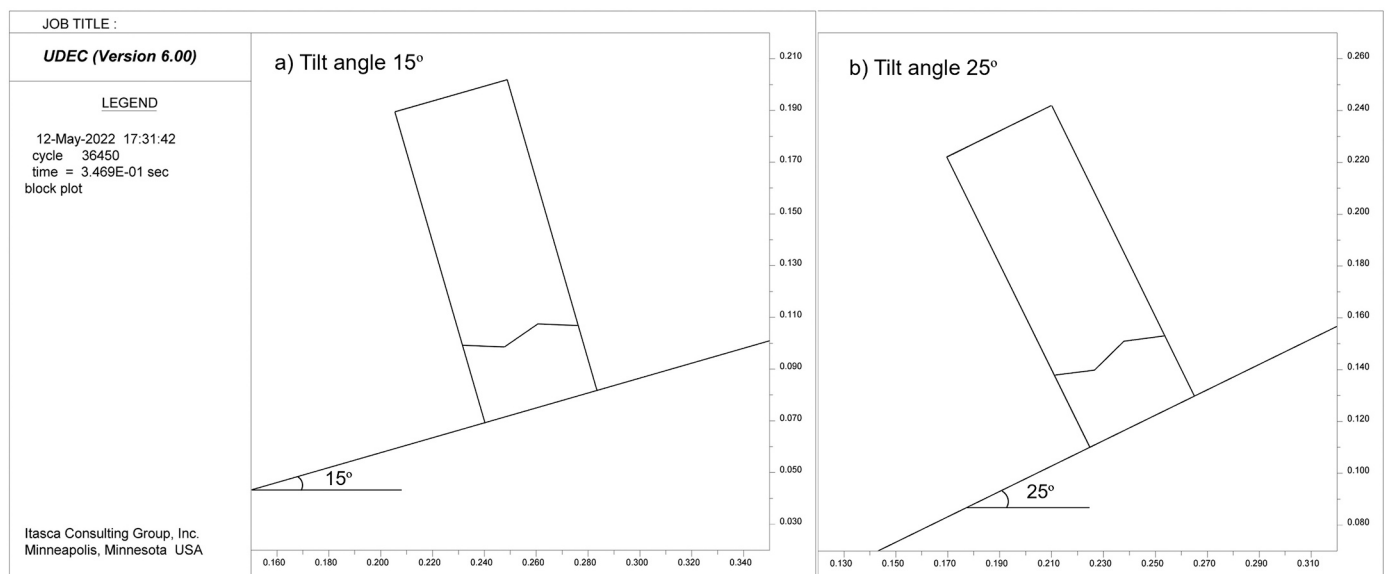


Fig. 4. Blocks located on a platform with different inclination angles (15° and 25°). The numerical models carried out in this study consist in preparing the models with increasing angles and check the instability mechanism (sliding or toppling) and the critical angle or angle at which the block model first topples or slides.

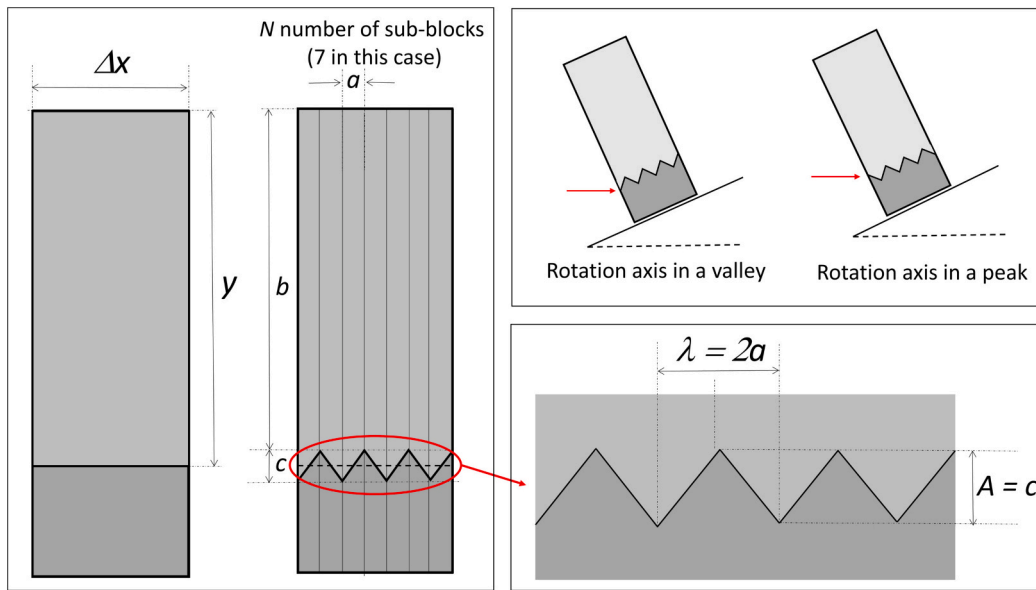


Fig. 5. Geometrical information concerning the preparation of samples for testing, considering a sample formed by 7 individual sub-blocks for illustrative purposes.

4 individual elements) or asymmetric (for 3) blocks. Regarding their geometry, N refers to the number of sub-blocks, a to the width of the individual sub-blocks, b to the smaller height of the individual sub-block and c to the difference between the larger and smaller heights of the individual sub-block. This produces assembled blocks of width Δx equal to $N \cdot a$, and average height y equal to $b + c/2$. Regarding the regular roughness, the amplitude A will be equal to c and the wavelength λ equal to $2a$, as depicted in Fig. 5. All blocks have a constant section $d = 20$ mm.

The prepared samples, named blocks A to G are illustrated in Fig. 6 and they include asymmetric and symmetric blocks. Every sample can be geometrically divided into several rectangles and triangles for computation purposes. Based on the geometric relations mentioned above, the geometry of every generated sample can be accurately measured and the results are presented in Table 1.

For samples formed by an uneven number of sub-blocks (such as 3, for samples A, B and E), the block can be tilted in such a way that the rotation points are located at a peak or a valley. For an even number of blocks (such as 4, for samples C and D or 2, for samples F and G), the rotation point will be located either at a valley (for concaves base samples such as C and F) or at a peak (for convex base samples such as D and G).

All these samples have been tilt tested to measure the critical angle of toppling or sliding of the blocks. They were tested three times in every direction until the instability was observed and the results were recorded to be compared with theoretical and numerical ones.

3.2. Surface roughness and estimates of geometrical JRC

Computing or estimating roughness is not a straightforward matter (Barton, 1973; Barton and Choubey, 1977; Tse and Cruden, 1979). Roughness is indeed a feature difficult to quantify by a single or a limited number of parameters and many different approaches can be used to do this. Moreover, rock mechanics studies have focused on quantifying roughness in terms of the mechanical response it produces, instead of in geometrical terms.

Early attempts to explain and predict the shear strength of non-planar rock joints (Patton, 1966) focused on the observed dilatant behaviour of granular materials and rough surfaces, and proposed Eq. (6) for the shear strength (τ) of a rock-joint at low normal stresses:

$$\tau = \sigma_n \tan(\phi_b + i) \quad (6)$$

Where σ_n is the effective normal stress, the angle i , also named effective roughness, is the average angle of deviation of displacement from the direction of the applied shear stress, and ϕ_b was the basic angle of friction of the rock that can be obtained through tilt tests on planar saw-cut rock surfaces (Alejano et al., 2018b).

For perfectly regular rough surfaces (Fig. 5), “ i ” can be computed as the dip of the regular teeth, that is:

$$i = \tan^{-1} \left(\frac{A}{\lambda/2} \right) = \tan^{-1} \left(\frac{c}{a} \right) \quad (7)$$

We will use this effective roughness or “ i ” angle value to quantify the regular roughness of the discontinuities artificially created for this study. However, other parameters are defined below with the aim of extending our study to irregularly rough based blocks in the future and clarifying the roughness characterization parameters.

Joint Roughness Coefficient (JRC) is a purely empirical and mechanical (non-geometrical) parameter, first introduced by Barton (1973) to fit a curvilinear strength criterion to rock joints according to Eq. (8).

$$JRC = \frac{\tan^{-1}(\tau/\sigma_n) - \phi_b}{\log_{10} \left(\frac{JCS}{\sigma_n} \right)} \quad (8)$$

Where JCS is the uniaxial compressive strength of the joint walls. Later, Barton and Choubey (1977) attempted to select the most typical geometrical profiles that produce equivalent JRC mechanical values based on tests in the lab (Fig. 7.a). These profiles (Fig. 7.a) are now widely used to quantify joint roughness in field and lab studies in an estimative manner. This parameter is also recommended for field rock mass characterization (ISRM, 2007). Remark that still JRC is a mechanical parameter, even if it is often quantified based on geometrical grounds.

Barton and Choubey (1977) also proposed to obtain JRC from field tilt tests based on the sliding angle (α) of the test and the effective normal stress generated by the gravitational force acting on the upper half of the block (σ_{n0}) according to Eq. (9):

$$JRC = \frac{\alpha - \phi_r}{\log_{10} \left(\frac{JCS}{\sigma_{n0}} \right)} \quad (9)$$

Remark that they changed in this proposal ϕ_b , related to intact rock to ϕ_r , the residual friction angle to account for potential weathering and

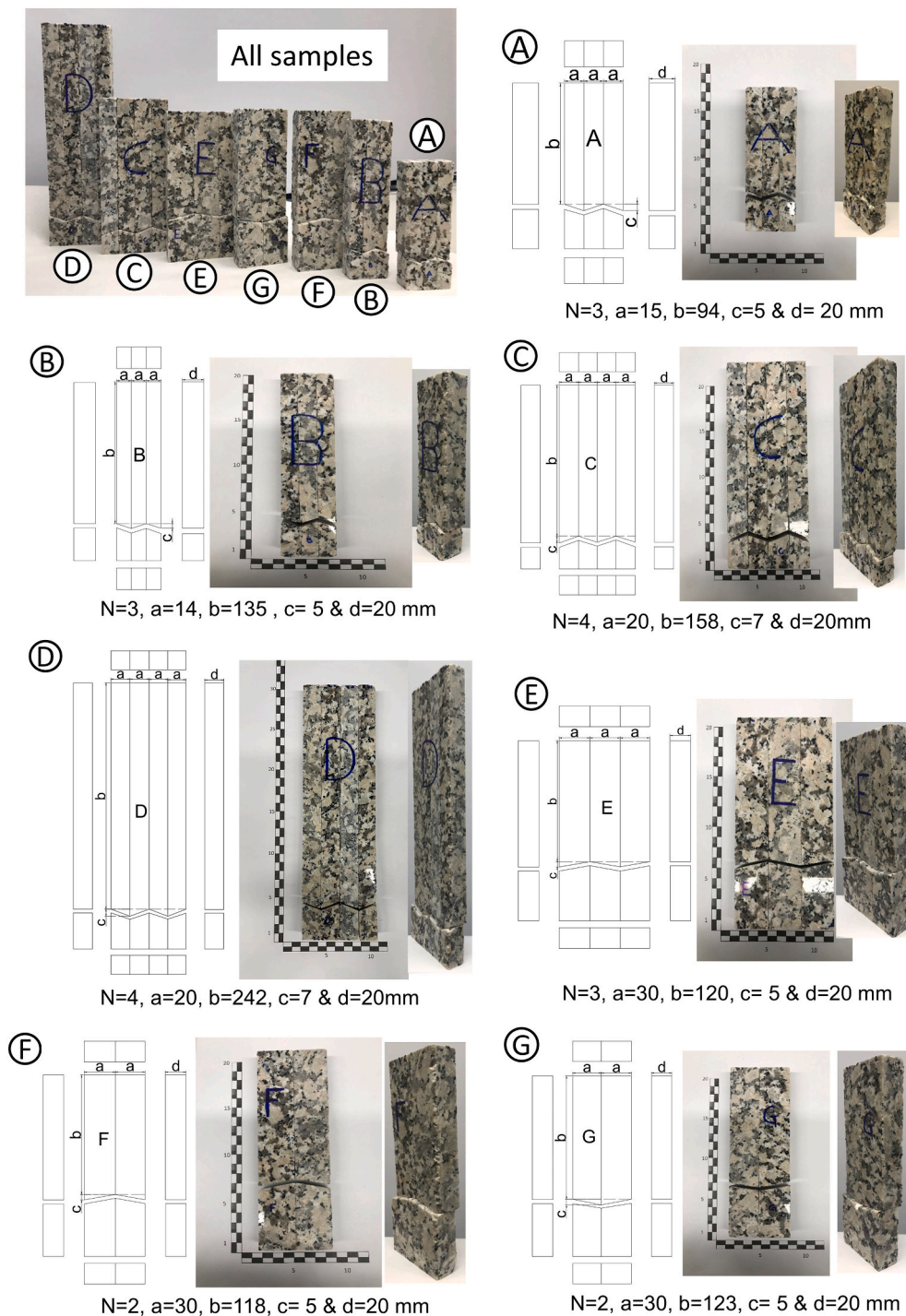


Fig. 6. Engineered granite blocks with a regular rough base. The values of the geometrical parameters are presented for every block.

Table 1
Geometrical parameters of the physical model blocks prepared.

Models	Type	<i>N</i>	<i>a</i> (mm)	<i>b</i> (mm)	<i>c</i> (mm)	Δx (mm)	<i>y</i> (mm)	<i>A</i> (mm)	λ (mm)
A	Peak-valley	3	15	94	5	45	96.5	5	30
B	Peak-valley	3	14	135	5	42	137.5	5	28
C	Valley (convex)	4	20	158	7	80	161.5	7	40
D	Peak (concave)	4	20	242	7	80	245.5	7	40
E	Peak-valley	3	30	120	5	90	122.5	5	60
F	Valley (convex)	2	30	118	5	60	120.5	5	60
G	Peak (concave)	2	30	123	5	60	125.5	5	60

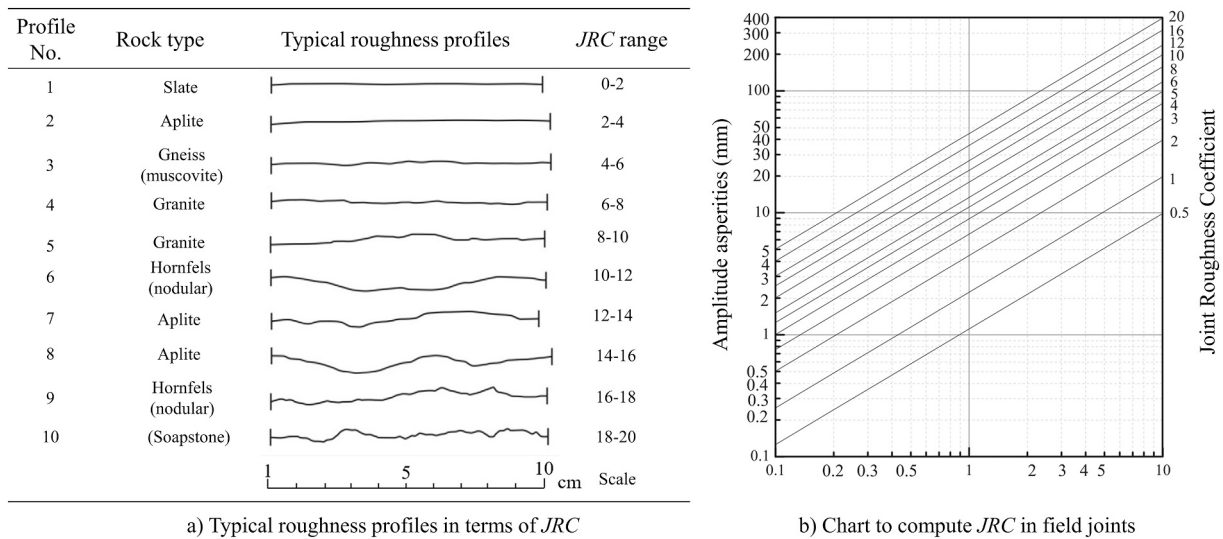


Fig. 7. a) Typical roughness profiles to estimate JRC in the field according to Barton and Choubey (1977); b) Chart to estimate JRC starting from the length and the amplitude of a profile based in Barton (1981).

polishing conditions of the joint walls. For our samples, the average value of the lab-measured basic friction angle is 30°, but due to repetitive testing and variability, the actual residual friction angle of the contacts can be in the range between 24° and 31°.

For regular surfaces, we can consider that $\alpha-\phi_r$ will be logically equal to the effective roughness “i” and for our regular rough samples Eq. (10) stands.

$$JRC = \frac{i}{\log_{10} \left(\frac{JCS}{\sigma_{n0}} \right)} \quad (10)$$

Barton (1981), based on the analysis of 200 specimens with a length of 0.1 m and some more on larger replicas, proposed a method to estimate JRC based on the length of the profile L and amplitude of the joint A, as in Eq. (11).

$$JRC \cong k \cdot A / L \quad \text{where} \quad \begin{matrix} k = 400 & \text{for } L = 0.1 \text{ m} \\ k = 450 & \text{for } L = 1.0 \text{ m} \\ k = 500 & \text{for } L = 10 \text{ m} \end{matrix} \quad (11)$$

He also provided a chart (Fig. 7.b) to compute the corresponding JRC for different joint geometries, widely used in practice in combination with Barton's comb.

The authors have obtained in Eq. (12) a rough estimative equation that can represent the values proposed in the Barton (1981) chart.

$$JRC = \frac{1}{2.05} \frac{A(mm)}{L(m)^{0.917}} \quad (12)$$

This approach can be acceptable for large discontinuities as those found in the field, but the scale does not adapt to the small artificial discontinuity sizes at stake.

With the aim of avoiding the subjectivity of estimates of JRC by comparison with typical profiles, Tse and Cruden (1979) analysed different correlations between geometrical roughness parameters and JRC. They eventually found that one of the most suitable ones was Z₂ as defined by Myers (1962), which refers to the root mean square of the first derivative of a two-dimensional profile under scrutiny:

$$Z_2 = \frac{1}{L} \int_{x=0}^{x=L} \left(\frac{dy}{dx} \right)^2 \quad (13)$$

Where L is the length of the profile and x and y its coordinates. The best fit found by Tse and Cruden (1979) for JRC was:

$$JRC = 32.2 + 32.47 \cdot \log Z_2 \quad (14)$$

With the aim of studying toppling on regular rough sources subjected to very low normal stresses, we have resorted to JRC approaches as presented in Eqs. (10), (12) and (14) to obtain estimative roughness of our samples. To compute this, the detailed geometry of every block is accounted for and the relevant geometrical and mechanical parameters (including V, volume; ρ, density; W, weight of the block; S, contact area; σ_n, normal stress and i, effective roughness) are reported in Table 2 with the corresponding JRC results.

Different approaches produce quite different results for our samples. The reasons behind the discrepancies are, all in all, associated with the mechanical focus of JRC. In this way, Eqs. (11) and (12) apply to large-scale discontinuities rather than to smaller ones and Eqs. (13) and (14) were developed based on natural regular profiles, which can be digitalized into numerous segments. Both of them though resort ultimately to the mechanical response to quantify JRC.

Therefore, for the samples (A-G) studied in this paper, we will use the effective roughness “i” as the reference roughness parameter. However, we suggest resorting to JRC computed as in Eq. (10) as a reference value, in case we want to extend the presented results to irregular rough surfaces as those often found in nature.

Moreover, we will later show how the main relevant parameter in terms of toppling response in relation to roughness of joints is the ratio A/γ, that is, the amplitude of the surface roughness in relation to block height. λ/Δx will only affect block widths below the roughness wavelength, which are difficult to find in practice.

4. Stability against toppling of slab-like blocks resting on tilted regularly rough bases

In case the base of a block is a rough surface, this roughness does affect its stability. In section 2, we introduced simple-geometry analytical expressions for blocks resting on tilted bases and we explained how it was possible to compute through other approaches. The idea is to extend these approaches to different blocks presenting roughness features that determine their mechanical response to toppling focusing on the samples illustrated in Fig. 6.

4.1. Analytical formulations

The authors have worked out the equations to compute factors of safety (FoS) and critical angles of toppling for the blocks prepared. To do that, the corresponding moment calculations have been adapted for the

Table 2
JRC values of models A-G calculated by Eqs. (10), (12) and (14).

Models	Rotation axis	V (cm ³)	ρ (g/cm ³)	W (N)	S (cm ²)	σ _n (kPa)	i (°)	JCS (MPa)	JRC (Eq. (10))	JRC (Eq. (12))	JRC (Eq. (14))
A	Peak-valley	86.85	2.64	2.25	9.0	2.29	18.4	120	3.9	41.9	16.7
B	Peak-valley	115.50	2.64	2.99	8.4	3.43	19.6	120	4.3	44.6	17.7
C	Valley	258.40	2.64	6.68	16.0	3.88	19.3	120	4.3	34.6	19.4
D	Peak	392.80	2.64	10.16	16.0	6.12	19.3	120	4.5	34.6	19.4
E	Peak-valley	220.50	2.64	5.70	18.0	2.83	9.5	120	2.0	22.2	6.9
F	Valley	144.60	2.64	3.74	12.0	2.92	9.5	120	2.1	32.2	6.9
G	Peak	150.60	2.64	3.89	12.00	2.97	9.5	120	2.1	32.2	6.9

different available blocks, by subdividing them into triangular or rectangular individual elements and different possible positions of the rotation axis (peak or valley). Blocks were assumed to present perfect edge corners. The detailed calculations are presented in Appendix A. The formulae obtained are compiled in Fig. 8 for each type of block and position (peak and valley), depending on the geometrical parameters used to prepare the block, namely *a*, *b* and *c*.

On the other hand, Alejano et al. (2015) realized that when preparing small rock blocks and subjecting them to tilt tests in the lab, the critical toppling angle tended to be somewhat smaller than computed. This was associated to the irregularities produced in the block edges in the cutting process. In fact, the saw-cut blocks have no perfectly sharp edges or corners, but irregular, and this irregularity is mechanically equivalent to consider the blocks having rounded edges, particularly in that acting as a rotation axis.

Accordingly, for blocks with rough bases, the irregularities of the edges may also play a relevant role in stability. Alejano et al. (2015) showed how to compute the stability of a block with rounded corners against toppling, both in terms of the factor of safety affected by this radius of curvature and on a critical angle (Eqs. (3) and (4)).

To account for this effect of irregularities in blocks with rough bases, the authors have also computed the toppling factors of safety and critical angles for the case of blocks at stake. In the case of blocks with square corners, the equivalent radius of curvature is the only parameter affecting the calculations. However, in blocks with non-square corners (this study), it is necessary to know not only the curvature radius but also the angle of the corner affected and if the rotation axis is located in a peak or a valley of the rough surface (Fig. 9).

As shown in Fig. 9, *r* refers to the distance between the position of the rotation point for a sharp edge and the new rotation point for round corner and *r_c* is the radius of the equivalent round corner. Additionally, an angle is needed for the calculations: δ_{*p*} (= *i* effective roughness),

which is the angle of roughness of the sub-triangle for toppling around a peak rotation axis or δ_{*v*} (= 90-*i*) the complementary angle of effective roughness for toppling around a valley axis. The corresponding computations are presented in due detail in Appendix B and the equations to compute the radius of curvature needed to produce toppling at a particular critical angle for the different possible geometries of blocks tested are presented in Fig. 10.

Here, the curvature radii of blocks E-valley and F are not included, since they did not show toppling. Therefore, for the case of block E, only for the peak rotation axis, the radius of curvature is considered.

In order to analytically study the stability of samples A to G illustrated in Fig. 6, based on the limit equilibrium method, it is possible to apply the analytical formulae developed in Appendices A and B and presented in Figs. 8 and 10.

4.2. Physical models

An experimental program was designed to study the stability in terms of factor of safety or the critical angle against toppling of rock blocks with regularly rough discontinuity bases subjected to tilt tests under laboratory conditions. The idea was to test the mechanical response of the blocks presented in section 3.1.

The tilt tests are carried out on a tilt table, where blocks are placed and the lower part of each block is fixed on the platform (Fig. 3). Then, the tilting table is progressively tilted until the upper part of the block topples or slides (as shown in Fig. 11). The tilting velocity for all tests is set constant and equal to 20°/min, following similar procedures as for basic friction angle estimates via tilt-tests (Alejano et al., 2018b). All the samples are tested three times until toppling or sliding is observed. The result is the average of the three values recovered. The physical records are compared with the analytical and numerical ones below.

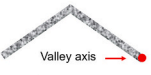
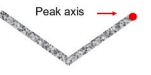

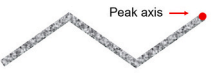

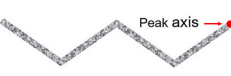
Shape of base	N	Block	Rotation axis	Equation
	2	F	Valley	$\alpha_{crit.} = \tan^{-1}\left(\frac{6ab + 3ac}{3b^2 + 6bc + 2c^2}\right)$ (A1.20)
	2	G	Peak	$\alpha_{crit.} = \tan^{-1}\left(\frac{6ab + 3ac}{3b^2 - c^2}\right)$ (A1.24)
	3	A, B, E	Valley	$\alpha_{crit.} = \tan^{-1}\left(\frac{27ab + 13ac}{9b^2 + 18bc + 6c^2}\right)$ (A1.8)
	3	A, B, E	Peak	$\alpha_{crit.} = \tan^{-1}\left(\frac{27ab + 14ac}{9b^2 - 3c^2}\right)$ (A1.4)
	4	C	Valley	$\alpha_{crit.} = \tan^{-1}\left(\frac{12ab + 6ac}{3b^2 + 6bc + 2c^2}\right)$ (A1.12)
	4	D	Peak	$\alpha_{crit.} = \tan^{-1}\left(\frac{12ab + 6ac}{3b^2 - c^2}\right)$ (A1.16)

Fig. 8. Roughness geometry sketches, for the different types of blocks and positions of the rotation axis, and critical angle equations for the different types of blocks as computed in Appendix A.

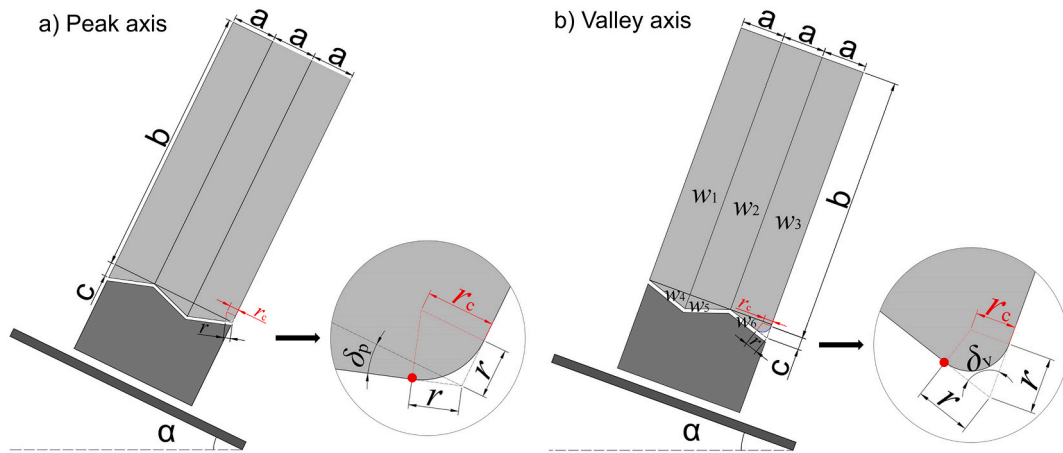


Fig. 9. Blocks with round corner of different equivalent radii: a) peak axis; b) valley axis.

Block	Rotation axis	Equation
A, B, E	Peak	$r_c = \frac{27ab + 14ac + (3c^2 - 9b^2) \tan \alpha_{phys.}}{(18b + 9c)(\cos \delta_p + \sin \delta_p \tan \alpha_{phys.})} \cdot \tan \left(\frac{\delta_p + 90^\circ}{2} \right) \quad (A2.6)$
	Valley	$r_c = \frac{27ab + 13ac - (9b^2 + 6c^2 + 18bc) \tan \alpha_{phys.}}{(18b + 9c)(\sin \delta_v - \cos \delta_v \cdot \tan \alpha_{phys.})} \cdot \tan \frac{\delta_v}{2} \quad (A2.11)$
C	Valley	$r_c = \frac{4ab + 2ac - \tan \alpha_{phys.} \cdot (b^2 + \frac{2}{3}c^2 + 2bc)}{(\sin \delta_v - \cos \delta_v \cdot \tan \alpha_{phys.}) \cdot (2b + c)} \cdot \tan \frac{\delta_v}{2} \quad (A2.16)$
D	Peak	$r_c = \frac{12ab + 6ac + (c^2 - 3b^2) \tan \alpha_{phys.}}{(6b + 3c)(\cos \delta_p + \sin \delta_p \tan \alpha_{phys.})} \cdot \tan \left(\frac{\delta_p + 90^\circ}{2} \right) \quad (A2.21)$
G	Peak	$r_c = \frac{6ab + 6ac + (c^2 - 3b^2) \tan \alpha_{phys.}}{(6b + 3c)(\cos \delta_p + \sin \delta_p \tan \alpha_{phys.})} \cdot \tan \left(\frac{\delta_p + 90^\circ}{2} \right) \quad (A2.26)$

Fig. 10. Equations for computing the radius of the corners that will produce the instability of the block for predetermined critical angle. These equations are developed in Appendix B.



a) Toppling in peak direction

b) Sliding in valley direction

Fig. 11. Physical model tests for block E, where the failure mechanism can be observed E: a) toppling with peak axis; b) sliding in valley direction.

4.3. Numerical models

UDEC (ITASCA Cons. Group Inc, 2014) is a 2D code based on the

discrete element method, so it can be used to solve differential stress-strain equations that control the behaviour of assemblies of rigid or deformable blocks. This code has been successfully used to study the

failure mechanisms of jointed rock masses, and particularly to analyse the toppling of rock blocks (Alzo'ubi, 2009; Alejano, 2021).

For this study, all blocks are modelled as rigid blocks, so no deformation can occur within them. Only relative movements of blocks can be reproduced, which represent the typical conditions of toppling in the field and in the physical models presented. The block representing the tilting table and the base block are always fixed (displacement totally restrained). Regarding geometrical conditions and in order to represent perfect geometrical blocks, a curvature radius $r = 1e-7$ m was used. The numerical procedure consisted in preparing the model with a particular tilt angle and running it subjected to gravity to check if the block remains stable or if it topples or slides. Various trials are run for different tilting angles to identify the smaller tilt angle at which each block becomes unstable.

Models are prepared to represent the corresponding regular roughness and block geometries, and input data files are created representing increasingly tilted bases. The block is located on a platform with the lower regular rough fixed base (Fig. 12). Based on initial estimations and after some trials as with planar contacts, the normal and shear contact stiffnesses are set to $k_n = 10^3$ GPa/m and $k_s = 10$ GPa/m, respectively. The friction angle (ϕ) of the contacts used in these numerical models is 30° as tested in the lab according to standards (Alejano et al., 2018b). This implies that, generally, we will observe sliding mechanisms for tilt angles around $\phi + i$, with i as in Table 2, in case this value is smaller than the critical toppling angle. This will not hold for blocks F and E-valley. For block F, this angle will be $\phi - i$, and for block E in the valley position a complex mechanism arise. These exceptions will be discussed in more detail in section 4.5.

UDEC contemplates the use of rounded corners (with a radius r) on blocks modelled to avoid bifurcation processes in the calculation procedure. For all the simulations carried out in this section, this radius is fixed at $1e-7$ m to represent sharp edge blocks.

Tentatively trying different models with various increasing tilt angles in intervals of 0.1° , the critical toppling/sliding angle corresponds to the lowest value at which an instability mechanism occurs.

Fig. 12 illustrates the simulations carried out to analyse the response of sample A for an initial position of the rotation axis in a peak (Fig. 12.a) and in a valley (Fig. 12.b). Models were carried out for different lower tilt angles until, at the presented cases the upper block toppled, which occurred in the peak case for a tilt angle of 26.2° and in the valley case for a tilt angle of 23.9° .

Toppling was not observed in all cases. For instance, for the simulation of sample E (Fig. 13), it occurs for a tilt angle of 37.4° when the sample was in a peak position (Fig. 13a). However, when the sample was in a valley position, a complex mechanism involving sliding arises instead of toppling for a tilt angle of 26.7° (Fig. 13b). This sliding response was also observed in the corresponding physical experiment (Fig. 11b).

It is relevant to remark that, as this case of block E shows, the fact that a block has a rough surface can affect the potential instability mechanism, in such a way that the location of the rotation axis (peak or valley) may produce a different response. This issue is not usually accounted for when analysing the stability of blocks against toppling or sliding and it will be commented in the discussion section.

After performing all the numerical simulations of the critical angle of toppling or sliding, numerical results are illustrated in Table 3, together with the analytical and physical model outcomes.

4.4. Analysis of results

Table 3 compiles the obtained results. The following comments are related to all blocks but F and E-valley. The first observation to be made is that the stability of the blocks is basically the same for the analytical and numerical results, with minor inaccuracies of less than 0.1° for all cases where toppling is observed. Therefore, the numerical results can be considered as validated for the scope of this study.

The second observation is that physical results are smaller, typically 2° to 4° , than the estimated value according to analytical or numerical approaches. This smaller value is attributed to irregularities in block edges, which can be analysed in terms of corner rounding.

For the asymmetrical samples (A, B and E), the difference between the case presenting the axis in a peak or a valley is about $3-4^\circ$ for the samples with i around 10° . In sample E this difference cannot be computed because for the valley position the sample slides, as explained below.

In previous studies, irregular and slightly rounded corners of the saw-cut sub-elements were typically observed when preparing the lab samples. This affects the stability response of these block models (Alejano et al., 2015). For instance, as illustrated in Table 3, the block C with a sharp edge would topple at 25.4° , but in the physical model, it topples at 21.7° . Based on the analytical approach considering round corners from Appendix B and shown in Fig. 9, it is possible to compute the

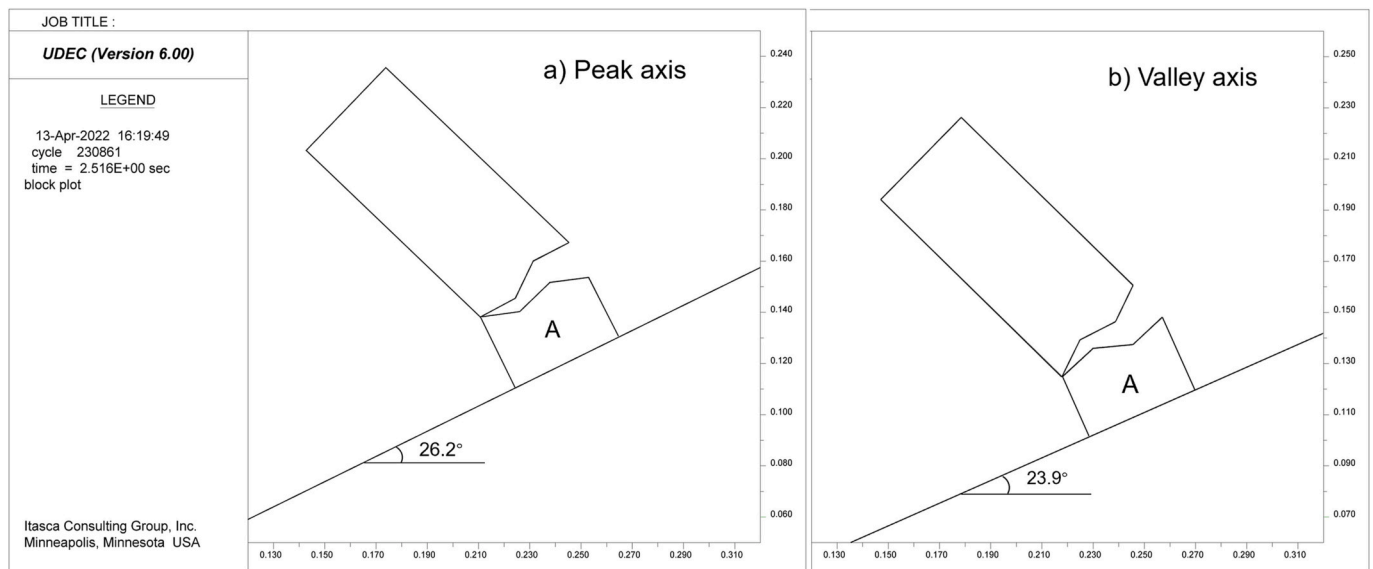


Fig. 12. Numerical modelling UDEC results of evolution of block A in tilt tests when positioning the block in such a way that the potential rotation axis is in a) a peak and b) a valley.

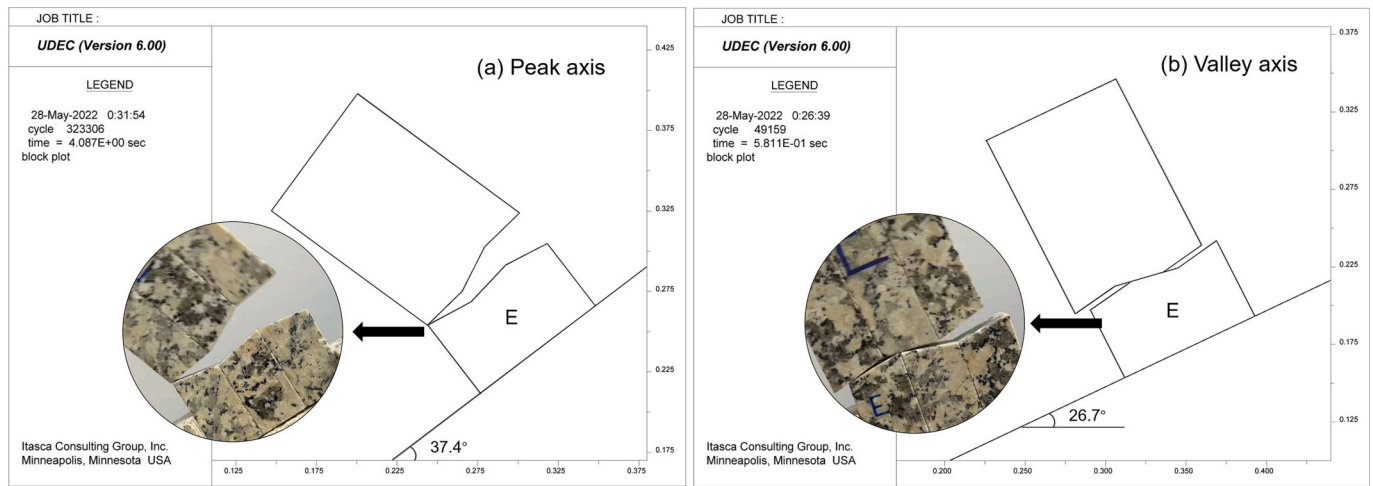


Fig. 13. Numerical simulation of block E: a) topples with peak axis; b) slides with valley axis.

Table 3

Critical toppling or sliding angles of the tested samples according to analytical solutions (Fig. 8), tilt tests and numerical models.

Models	Position of rotation axis	i (°)	α_{slide} (°) = $\phi_b + i$	α_{ana} (°)	α_{phys} (°)	α_{num} (°)
A	Peak	18.4	48.4	26.2	23.5	26.2
	Valley	18.4	48.4	23.9	19.8	23.9
B	Peak	19.6	49.6	17.6	15.0	17.6
	Valley	19.6	49.6	16.4	12.6	16.4
C	Valley	19.3	49.3	25.4	21.7	25.3
	Valley	19.3	49.3	25.4	21.4	25.3
D	Peak	19.3	49.3	18.5	15.3	18.5
	Peak	19.3	49.3	18.5	15.1	18.5
E	Valley	9.5	39.5	35.2	26.7*	27.5*
	Peak	9.5	39.5	37.5	37.4	37.4
F	Valley	9.5	20.5	25.6	20.5*	20.5*
	Valley	9.5	20.5	25.6	20.5*	20.5*
G	Peak	9.5	39.5	26.5	23.8	26.4
	Peak	9.5	39.5	26.5	23.9	26.4

* The observed mechanism is sliding.

equivalent radius of curvature that will produce the critical angle observed in the physical models. These equivalent radii for the toppling blocks (sliding results are removed) are presented in Table 4.

The computed rounding value is generally in the range of 3 to 6 mm, except for block D where large irregularities are detected.

As it can be observed, the occurrence of irregular corners tends to make the real blocks less stable than computed theoretically for straight

Table 4

Analytical and physical critical angles for the toppling samples and equivalent curvature radius analytically computed (Fig. 10) to produce the observed results. Also, the analytical FoS corresponding to the observed failure physical critical angle is computed.

Models	Position of rotation axis	α_{ana} (°) (Individual formula)	α_{phys} (°)	α_{num} (°)	r_c (mm)	FoS for α_{phys}
A	Peak	26.22	23.5	26.2	3.36	1.13
	Valley	23.89	19.8	23.9	3.61	1.23
B	Peak	17.60	15.0	17.6	4.49	1.18
	Valley	16.41	12.6	16.4	4.12	1.32
C	Valley	25.40	21.7	25.3	5.66	1.20
	Valley	25.40	21.4	25.3	6.09	1.21
D	Peak	18.54	15.3	18.5	10.06	1.22
	Peak	18.54	15.1	18.5	10.68	1.25
E	Peak	37.48	37.4	37.4	0.13	1.00
G	Peak	26.47	23.8	26.4	3.82	1.13
	Peak	26.47	23.9	26.4	3.68	1.13

corners. This induces a decrease in factor of safety of about 0.15 to 0.2 units on average for the small blocks tested. For some actual larger rock blocks in the field, it is estimated that this effect could be even more relevant (Pérez-Rey et al., 2019).

4.5. Relevant considerations

Three methods, including theoretical analyses, physical tests and numerical models, were used to understand block toppling on rough base surfaces. Analytical and numerical results coincide. Physical results are also similar, being the observed differences attributed to imperfections generated in the cutting process, particularly relevant for the blocks with rougher surfaces ($i = 20^\circ$).

In physical tests and numerical models, block F and E-valley and F slid rather than toppled. The theoretically computed sliding angle is larger than the one observed. The observed behaviour is explained as follows for each case.

For block F, no contact between the upper right hand side sub-element and the base along down-dip direction occurs when tilted around 10° or more (normal stress was concentrated in the down-dip or left part of the base, according to Fig. 6.f). The analytical critical sliding angle is $\phi - i$ (20.5°), which is smaller than the analytical critical toppling angle 25.6° . When the tilt angle of both physical and numerical models gets to 20.5° , sliding in the down-dip or left part tends to occur, although due to the geometry this sliding is constrained. The energy of sliding makes the block to ultimately toppling. This means that the initial instability mechanism is sliding, but due to geometrical constraints after sliding some mm, then the block tends to topple around the external corner. The concentration of normal stress plays here a key role.

For block E, theoretically, the block will slide at the analytical critical angle 39.5° (toppling at 35.2° , if so). However, a complex phenomenon occurs. After some tilting there is no contact between the upper sub-elements along down-dip base of the right-hand side (Fig. 6.e), so most of the normal stress is concentrated in the intermediate sub-element. At 14.5° , the block tends to topple around the only peak point in the surface, but the whole block does not topple due to geometrical constraints: movement is limited in the left-hand side element. As tilting continues, the normal stress will be slowly transferred from the intermediate sub-element contact to the left one. This decrease in normal stress will produce a decrease in shear stress so that corresponding to sliding is attained in this intermediate contact, which will produce sliding when attaining 26.7° physically or 27.5° numerically. The block that slightly rotated at 14.5° , starts now to slide at about 27° and after some sliding run (Fig. 13.b, numerical and physical), it ultimately topples (Fig. 11-b, physical).

This kind of circumstances occur for blocks when the roughness wave-length is small (1 or 1.5 times) in relation to block width, which will be a case rather uncommon in practice. Theoretically, sliding will occur when the sum of the friction angle of the contact base plus the positive or negative angle of the saw-tooth face are larger than the dip angle when instability happens; but block movement can be constrained by geometry. Additionally, due to variation in normal forces in the contacts, irregularities in the shape of the contacts including irregular edges and surfaces polishing, it will be difficult to predict behaviour in these cases.

The experimental results tended to be smaller than the theoretical ones due to imperfections during cutting, resulting in some rounded edge effect of the blocks. This justifies the need of considering the equivalent curvature radius of saw-cut corners to obtain accurate results, according to formulae presented in Appendix B.

5. General equations of rock blocks with regular rough base

Based on the results observed for the tested blocks, we try to generalize the analytical approach, so it can be widely applied to any block resting on a regular rough surface and, additionally, to irregular rough based blocks, as usually found in nature. This general approach will be evaluated with the tested blocks and it will be analysed in some detail to obtain some relevant general conclusions.

5.1. General formulation to compute the stability of a block resting on a regularly rough base

The geometry of the prepared blocks was synthetically described through parameters N , a , b , and c . These parameters, useful for the preliminary calculations, are now used to compute more general geometrical and regular roughness parameters (Fig. 5) including Δx or block width, y or average block height, A or roughness amplitude, and λ or roughness wavelength.

The position of the rotation axis in relation to the amplitude of the

roughness is very relevant to analyse stability. The authors will focus on the mid-position equivalent to a non-rough base, formulated on previous calculations (Eqs. (1) and (2)) and, particularly, in the two extreme positions denoted as peak, the highest possible axis location rendering the most stable case, and valley, the lowest possible axis location representing the least stable condition.

The value N , representing the number of sub-elements needed to create the physical sample, can now be computed, based on the block width and the roughness wavelength, as $N = 2\Delta x/\lambda$. Similarly, simple equations can be used to derive all the initial simplified values N , a , b , and c , starting from the general parameters Δx , y , A , and λ or vice-versa.

It is relevant to note, at this point, that for homogenous blocks (equal density in the whole block), the scale of the block does not affect the toppling behaviour, so all homothetic blocks will behave in the same manner in relation to toppling response. Based on this consideration, and to generalize the computations, we have initially considered the parameters potentially affecting toppling results. They include the number of blocks (N), the inverse slenderness ($\Delta x/y$), the relative amplitude (A/y), and the relative wavelength ($\lambda/\Delta x$). Ranges of expectable values of these parameters have been selected as shown in Fig. 14. Ranges of $N = 2, 3, 4$ and 7 (even if this value was not finally computed), $\Delta x/y = 2/3, 1/2, 1/3$ and $1/5$, $A/y = 1\%, 2\%, 5\%$ and 10% and $\lambda/\Delta x = 1, 1/2, 1/5$, and $1/10$ were considered.

Considering that all the triangle elements over the contact are symmetric, such as in the cases for an even number of sub-blocks, it is possible to compute their effect in a simplified manner. The weight component of these triangles parallel to the contact line will produce overturning moments for the case of the rotation axis in the position of the valley and stabilizing moments for the case of the axis in a peak position. The arm of these moments will locate $1/6 A$ over the axis valley position in the first case, and $1/3 A$ below the axis peak position in the second, according to the position of the centre of gravity in a triangle.

Therefore, the equations were computed for the critical angles for the cases of peak axis position and valley axis positions (Fig. 15), and where it can be checked that null amplitude solutions ($A = 0$) converge to that

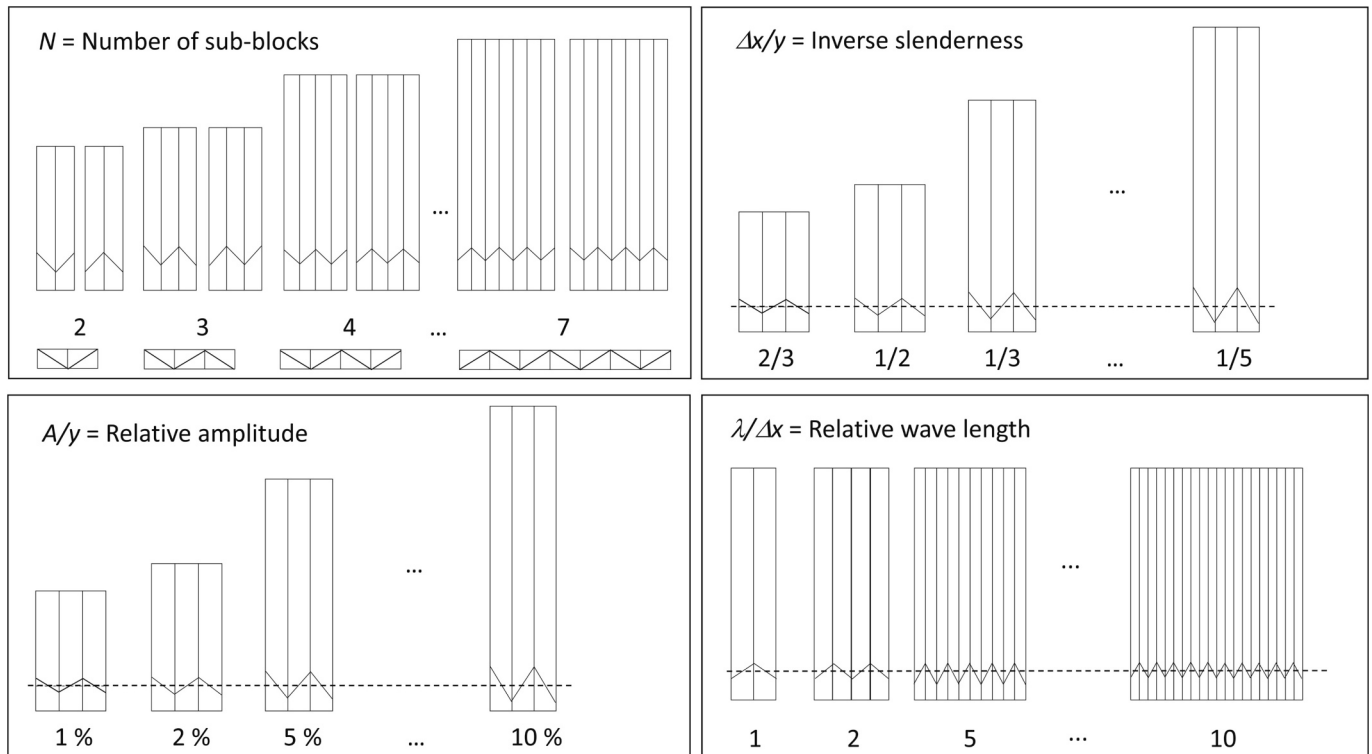


Fig. 14. Change in block morphology according to the four parameters considered for analysing results.

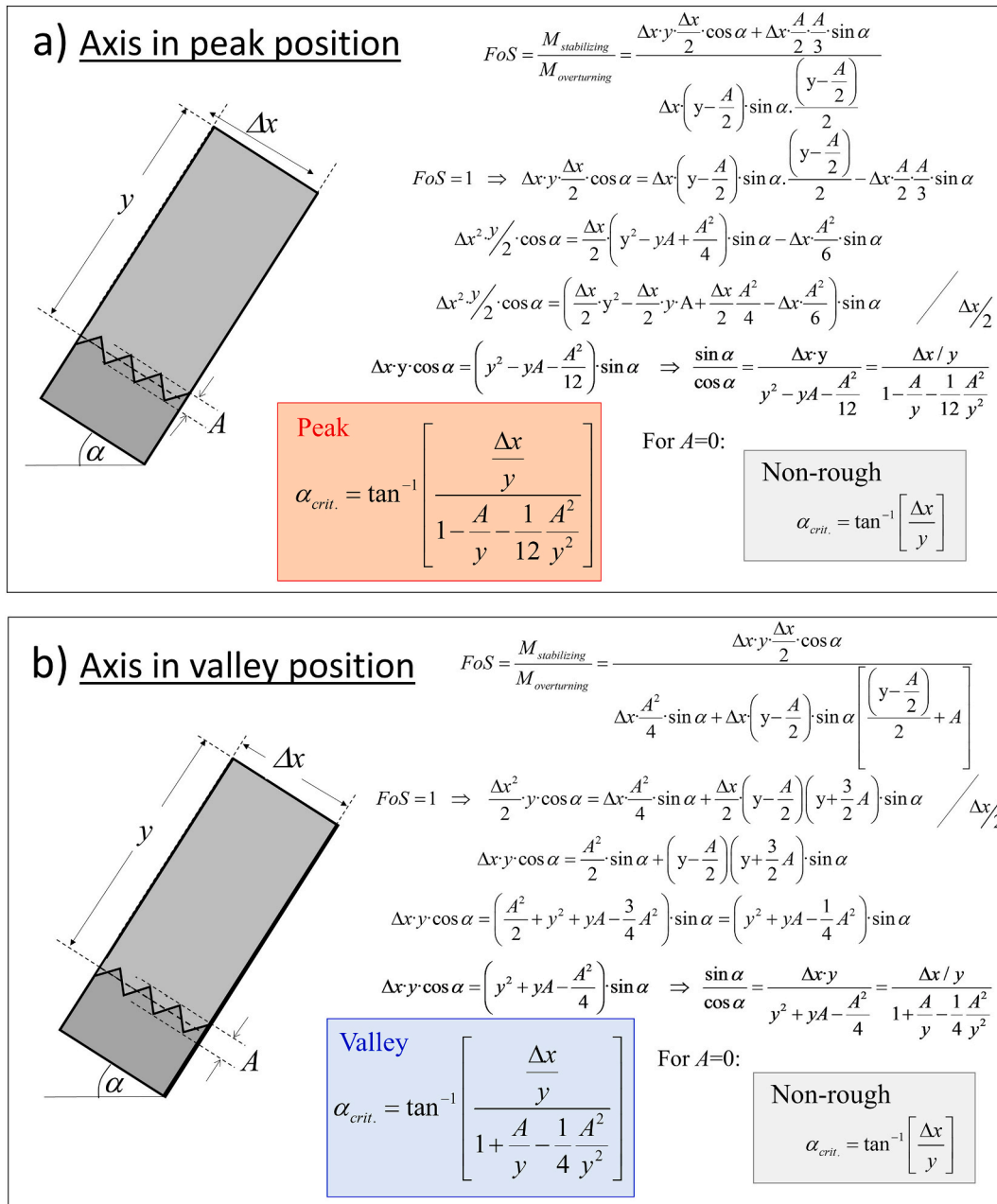


Fig. 15. General computation of the critical angle for blocks resting on a regular rough surface.

of a standard block with a planar base. Moreover, it can be checked that when applying these formulae to non-symmetric blocks, for instance, that showing 3 sub-blocks, the error made in the calculations is below 0.1°, usually below the measurement accuracy.

Based on the approach developed in Fig. 15, it is also possible to obtain general FoS formulations for toppling of blocks with regularly rough bases including the case of a block in the peak position (Eq. 15):

$$FoS_{peak} = \tan^{-1} \alpha \cdot \frac{\Delta x / y}{1 - \frac{A}{y} - \frac{1}{12} \frac{A^2}{y^2}} \quad (15)$$

And the FoS for the case of a block in the valley position (Eq. 16):

$$FoS_{valley} = \tan^{-1} \alpha \cdot \frac{\Delta x / y}{1 + \frac{A}{y} - \frac{1}{4} \frac{A^2}{y^2}} \quad (16)$$

Note that if the amplitude of roughness is set to 0 in any of these formulae (planar surface) the original Eq. (2) is recovered.

$$FoS = \tan^{-1} \alpha \cdot \frac{\Delta x}{y} \quad (17)$$

The individual formulae (section 4.1) are perfectly rigorous analytical expressions computed for every possible geometry of the prepared blocks. The general formulation was obtained as a good approximation that produces very low errors and that can be more suitable for practical application. For small wavelength roughness, there can be significant differences between individual and general approaches. For individual formulae, it has been possible to implement the effect of round corners, something not possible for the general approach.

5.2. Application of general formulae to tested blocks

The results obtained using these general formulae are highly consistent with the ones based on the original expressions shown in Table 5. The difference between the calculated toppling angles is below

Table 5

Critical angle for toppling blocks tested according to the individual block formulae, the general formulation and the numerical approach.

Models	Position of rotation axis	$\alpha_{ana.} (^{\circ})$ (General formula)	$\alpha_{ana.} (^{\circ})$ (Individual formulae)	$\alpha_{num.} (^{\circ})$
A	Peak	26.19	26.22	26.2
	Valley	23.92	23.89	23.9
B	Peak	17.59	17.60	17.6
	Valley	16.43	16.41	16.4
C	Valley	25.41	25.40	25.3
D	Peak	18.54	18.54	18.5
E	Peak	37.45	37.48	37.4
G	Peak	26.47	26.47	26.4

0.03° and, therefore, negligible for practical purposes. This general formulation works well for blocks with a regularly rough contact base and could ease the extrapolation to blocks with irregularly rough bases.

5.3. Considerations on the impact of roughness on the stability of blocks against toppling

Aiming at understanding the influence of the roughness (in terms of relative amplitude) on the potential toppling of blocks, we have represented in Fig. 16, the factors of safety of different individual blocks in relation to tilt angle. The graph illustrates the response in terms of factors of safety (FoS) related to tilt angle (α) of three possible simple geometry blocks (inverse slenderness or $\Delta x/y$ equal to 1/2, 3/4 and 1) considering the peak and valley positions for a large relative amplitude (A/y) of 10%.

In this graph, different aspects can be highlighted. First, the angle of toppling will be that corresponding to $FoS = 1$ for the planar surface case, namely 27° for inverse slenderness 0.5, 37° for 0.75 and 45° for 1. However, if a relative amplitude of 10% is considered, the potential variability between peak and valley positions will induce critical toppling angle for ranges up to nearly $\pm 3^{\circ}$, which can be rather relevant when analysing the stability of single blocks. For instance, the 0.75 inverse slenderness block could topple for an angle of 34.3° (for the valley case), but it could still stand until attaining the tilting surface at an angle of 40° (for the case of the rotation axis in a peak position).

Conversely, this potential variability associated with roughness and the position of the rotation axis will have a relevant impact on FoS

computations. Accordingly, we have highlighted in the graph three cases. The first one analyses the 0.5 inverse slenderness block on a surface tilted 20°; the standard FoS will be 1.37 but it will range between 1.25 for a valley axis to 1.53 to a peak axis always for a relative amplitude A/y of 10%. This variation of ± 0.15 units of FoS (roughly 30%) can take place in association with a rough base in a block. Similar values can be derived for other block slenderness as shown in Table 6.

Also in Table 6, the same cases are considered, with extreme (peak and valley) values associated with a 5% of relative amplitude, instead of the 10% used for the example in the graph. In this case, the variation diminishes to up to ± 0.1 units of FoS (roughly 20%), which can still induce important errors in instability estimates.

In conclusion, the computed formulation and the illustrative graph show how the fact of having a rough base can influence the stability of individual blocks against toppling.

6. Discussion

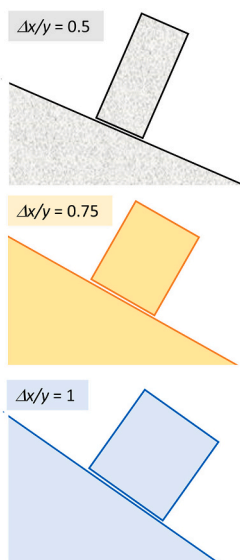
Failure mechanisms involving toppling are affected by natural discontinuities, whose geometry and geomechanical features can induce potential inaccuracies when analysing its stability in a simplistic manner. In nature, it is not difficult to find rock blocks prone to topple. This may endanger infrastructures, buildings and people's safety, so it is important to assess the stability of these blocks.

In the past decades, methods were proposed to analyse the stability of blocks against toppling, but there were still some open issues. In some cases, especially for those blocks with a relatively complex geometry and a rough base, it is still difficult to rigorously analyse its stability. The

Table 6
Examples of FoS against toppling variation for different situations.

Block	Inverse of slenderness $\Delta x/y$	Rel. amplitude A/y	Tilt angle $\alpha (^{\circ})$	FoS_{planar}	FoS_{peak}	FoS_{valley}
1	0.5	0.1	20	1.37	1.53	1.25
2	0.75	0.1	25	1.61	1.78	1.46
3	1	0.1	30	1.73	1.92	1.57
4	0.5	0.05	20	1.37	1.44	1.30
5	0.75	0.05	25	1.61	1.69	1.53
6	1	0.05	30	1.73	1.82	1.65

For relative amplitude (A/y) = 10%



Factor of safety values against toppling according to tilt angle for different slender blocks and base roughness

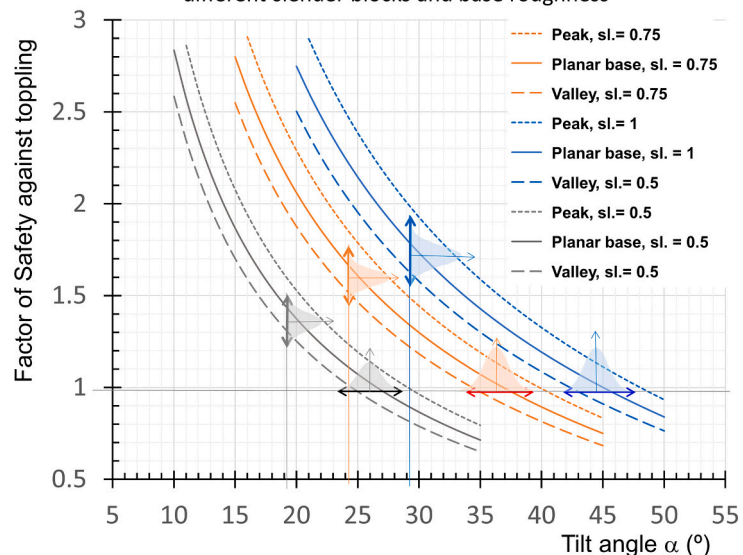


Fig. 16. Computation of factors of safety for three different slender blocks for planar, peak and valley positions according to Eqs. (15), (16) and (17).

presented study contributes to this endeavour, even if it is recognized that the appropriate estimation and application of the needed parameters is still difficult.

Based on the general equations of rock blocks with a regularly rough base presented in this study, it is possible to analyse the stability of a single rock block resting on a rough surface. Here, we consider only regularly rough bases, i.e., the regular saw-tooth contact base. Future work will advance towards extending this study to the case of blocks with irregular rough bases.

Based on the formulations provided and test results, *JRC* as typically used may not be suitable to study the role of roughness on toppling stability, since it was thought and developed to study the frictional behaviour, that controls sliding. Susceptibility to toppling is more related to the position of the centre of gravity of the rock block in relation to the rock block base, which can be affected by the position of the rotation axis and the relative amplitude of the base roughness.

Furthermore, the study of this paper can also be of help to produce more accurate stability estimates of stability of rock boulders (Fig. 17a and b) or other singular rock blocks (Fig. 17c and d). The last author studied the stability of a natural granite ellipsoidal boulder roughly 8-m length and 3-m height (Pérez-Rey et al., 2019), as shown in Fig. 17a, resting on a small contact area of about 0.6 m². The critical angle against toppling was estimated to be 31.4° for a planar contact, which is larger than the estimated dip angle 27°.

The boulder was computed to be stable in the current condition, both for sliding and toppling. If roughness on the contact could be estimated and accounted for and the location of the rotation axis known, this critical angle could be reduced or increased. Accordingly, for these blocks close to equilibrium, a good knowledge of the geometry of the contact and the presented equations could be of help to better assess and fine-tune stability computations.

To illustrate this, we resort to the classic stability graph for toppling and sliding of blocks initially proposed by Ashby (1971), and we consider 4 regular blocks whose slenderness and tilting angle position are as indicated in Table 7. Considering a planar block contact, all these blocks will slide, as illustrated in Fig. 18a. However, if we consider a rough base (with $A/y = 1\%$), the results are different. According to the formulation presented: block 1 will be stable; blocks 2 and 4 will be stable, but they will topple if the axis is in a valley position and block 3 will topple, but it will be stable, if the axis is in a peak position (Table 7, Fig. 18b). In conclusion, considering the roughness of a block base can be important to analyse its potential failure mechanism and stability.

7. Conclusions

Different types of toppling mechanisms occur in natural and mining slopes and road cuts in rock masses. The simplest mechanism of toppling involves one simple geometry block resting on a planar surface and already detached from the rest of the rock mass. This case was studied in

Table 7
Theoretical analysis of four blocks.

Block	Inverse of slenderness $\Delta x/y$	Tilt angle $\alpha(^{\circ})$	Stability planar base	Stability rough base
1	$> \tan(\phi_b + i)$	$\phi_b + 1$	Slides	Stable
2	$> \tan(\phi_b + i)$	$\phi_b + i - 1$	Slides	Stable, topples if valley
3	$\tan \phi_b < \Delta x/y < \tan(\phi_b + i)$	$\phi_b + i - 1$	Slides	Topples, stable if peak
4	$\tan \phi_b < \Delta x/y < \tan(\phi_b + i)$	$\phi_b + 1$	Slides	Stable, topples if valley



Fig. 17. a) View of the “Pena do Equilibrio” granite boulder in Pontearreas, Galicia, Spain, b) A similar but larger boulder in Matopos (Zimbabwe) c) Granite slab-like block prone to toppling and d) Two granite slab-like blocks already toppled, both these last cases at Monte Pindo, Galicia, Spain.

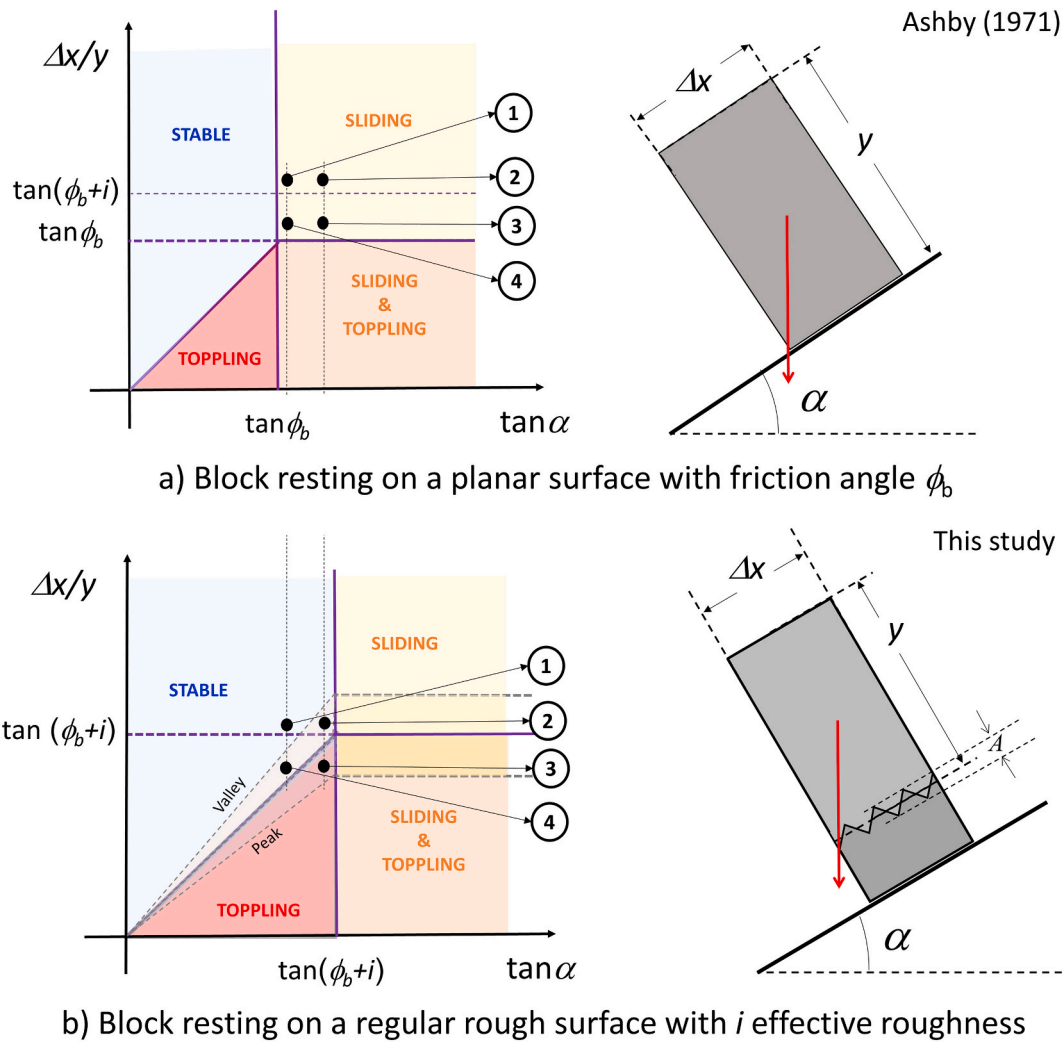


Fig. 18. a) Mechanism map of block stability for planar base blocks and b) Same map for blocks with a regular rough base.

the past for somewhat simple geometries, but the influence of a potential rough surface base has not been so far addressed.

The study builds on previous works where the stability of rock blocks of particular geometry was investigated. The toppling stability of a rock block resting on a regularly rough surface is then rigorously analysed by means of limit equilibrium analytical methods, physical tests with small saw-cut rock blocks and discrete element numerical models. The results of theoretical analyses, physical tests and numerical models are consistent, indicating that roughness does affect the toppling response.

Moreover, roughness can affect the type of instability mechanism to which a particular block is more prone to, either sliding or toppling. Certainly, for many actual rock blocks, the influence of roughness on the stability of blocks will be scarcely relevant. However, under some circumstances, roughness can play a relevant role. Therefore, it is convenient to have available tools to account for roughness within stability calculations against toppling, as those developed in this paper.

A general but simple formulation is proposed for computing the factor of safety against toppling of a block resting on a regularly rough surface. Slenderness and the relation of roughness amplitude to block height have shown to be the most relevant parameters. This formulation can be used to assess the potential influence of roughness on any particular scenario. This study ultimately contributes to a better understanding of the role of surface roughness on toppling-related

instabilities in rock masses.

Declaration of Competing Interest

The authors declare that they have no known competing financial interests or personal relationships that could have appeared to influence the work reported in this paper.

Data availability

Data will be made available on request.

Acknowledgement

The first author Jingyun Gui acknowledges China Scholarship Council (CSC) for her stay at the University of Vigo by means of a CSC grant number 202106560049. The second, third and fifth authors affiliated to the University of Vigo acknowledge the Spanish Ministry of Universities for partially funding this study as part of the project awarded under Contract Reference No. RTI2018-093563-B-I00, partially financed by means of ERDF funds from the EU. Funding for open access charge: Universidade de Vigo/CISUG.

Appendix A. Appendix

A.1. Individual equations for estimating the factor of safety and critical toppling angle of all the tested blocks (A-G)

In this study, the analytical computation of the factor of safety (FoS) against toppling is based on the limit equilibrium method, which relates the stabilizing and overturning moments related to a potential rotation axis, as stated in Eq. (1). The angle at which a particular block topples when resting on a tilted surface or, critical angle of toppling, can also be computed by equating FoS to 1. These values can be computed for any block by decomposing it into rectangle and triangle-shaped elements. The detailed individual computation for all the physical blocks prepared as shown in Fig. 7 and for the two possible directions of tilting including peak and valley rotation axes is presented in this Appendix A. Remark that for all computation, the rotation axis is located on the origin of the coordinate system.

A.1.1. Blocks A, B, and E rotating around a peak and a valley axis

It can be easily identified that blocks A, B, and E have similar geometry conditions assembled by saw-cut pieces, therefore, the following computations are suitable for all the three blocks. Blocks A, B and E are asymmetrical and can be divided into two situations including peak and valley axis.

In the case of a block with the rotation axis in a peak (Fig. A1.1a), the equation for estimating the FoS decomposing the block into its six sub-elements is as follows:

$$\begin{aligned} \sum M_{stabilizing} &= w_1 \cos\alpha \cdot \left(\frac{a}{2} + 2a\right) + w_2 \cos\alpha \cdot \left(\frac{a}{2} + a\right) + w_3 \cos\alpha \cdot \frac{a}{2} + \\ &+ w_4 \cos\alpha \cdot \left(\frac{2a}{3} + 2a\right) + w_5 \cos\alpha \cdot \left(\frac{a}{3} + a\right) + w_6 \cos\alpha \cdot \frac{2a}{3} + \\ &+ (w_4 + w_5 + w_6) \sin\alpha \cdot \frac{c}{3} \end{aligned} \tag{A1.1}$$

$$\sum M_{overturning} = (w_1 + w_2 + w_3) \sin\alpha \cdot \frac{b}{2} \tag{A1.2}$$

Where α is the dip of the tilting surface; w_i are the weights of the different sub-elements, a , b and c are specific lengths of the block (Fig. A1.1). Accounting for the fact that $w_1 = w_2 = w_3$ and $w_4 = w_5 = w_6$, the computation of the FoS can be simplified to:

$$FoS_{toppling} = \frac{c^2}{3b^2} + \left(\frac{27ab + 14ac}{9b^2}\right) \cdot \tan^{-1} \alpha \tag{A1.3}$$

Equating FoS to 1 for limit equilibrium, the critical angle for toppling in Fig. A1.1a can be derived:

$$\alpha_{crit.} = \tan^{-1} \left(\frac{27ab + 14ac}{9b^2 - 3c^2}\right) \tag{A1.4}$$

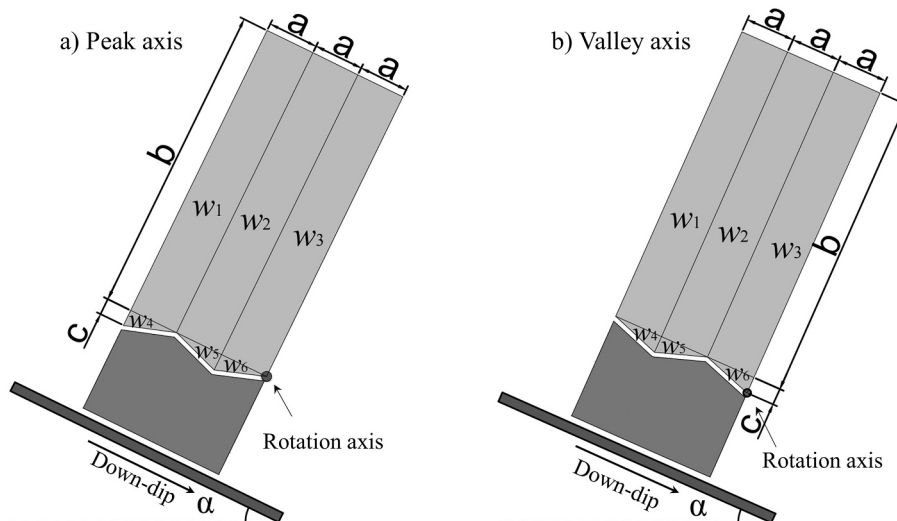


Fig. A1.1. a) Blocks A, B and E toppling with peak axis; b) block A, B and E toppling with valley axis.

Similarly, in the case of a block with a valley axis (as shown in Fig. A1.1b),

$$\begin{aligned} \sum M_{stabilizing} &= w_1 \cos\alpha \cdot \left(\frac{a}{2} + 2a\right) + w_2 \cos\alpha \cdot \left(\frac{a}{2} + a\right) + w_3 \cos\alpha \cdot \frac{a}{2} + \\ &+ w_4 \cos\alpha \cdot \left(\frac{a}{3} + 2a\right) + w_5 \cos\alpha \cdot \left(\frac{2a}{3} + a\right) + w_6 \cos\alpha \cdot \frac{a}{3} \end{aligned} \tag{A1.5}$$

$$\sum M_{overturning} = (w_1 + w_2 + w_3) \sin\alpha \cdot \left(\frac{b}{2} + c\right) + (w_4 + w_5 + w_6) \sin\alpha \cdot \frac{2c}{3} \tag{A1.6}$$

The simplified equation of FoS can be again obtained as:

$$FoS_{toppling} = \left(\frac{27ab + 13ac}{9b^2 + 18bc + 6c^2} \right) \cdot \tan^{-1} \alpha \tag{A1.7}$$

The toppling angle α_{crit} (Fig. A1.1b) can be computed as:

$$\alpha_{crit.} = \tan^{-1} \left(\frac{27ab + 13ac}{9b^2 + 18bc + 6c^2} \right) \tag{A1.8}$$

A.1.2. Block C rotating around a valley axis

Fig. A1.2a refers to the case where the block C rotates with a valley axis, and we obtain,

$$\begin{aligned} \sum M_{stabilizing} &= w_1 \cos \alpha \cdot \left(\frac{a}{2} + 3a \right) + w_2 \cos \alpha \cdot \left(\frac{a}{2} + 2a \right) + \\ &+ w_3 \cos \alpha \cdot \left(\frac{a}{2} + a \right) + w_4 \cos \alpha \cdot \frac{a}{2} + w_5 \cos \alpha \cdot \left(\frac{2a}{3} + 3a \right) + \\ &+ w_6 \cos \alpha \cdot \left(\frac{a}{3} + 2a \right) + w_7 \cos \alpha \cdot \left(\frac{2a}{3} + a \right) + w_8 \cos \alpha \cdot \frac{a}{3} \end{aligned} \tag{A1.9}$$

$$\begin{aligned} \sum M_{overturning} &= (w_1 + w_2 + w_3 + w_4) \sin \alpha \cdot \left(\frac{b}{2} + c \right) + \\ &+ (w_5 + w_6 + w_7 + w_8) \sin \alpha \cdot \frac{2c}{3} \end{aligned} \tag{A1.10}$$

Based on the fact that $w_1 = w_2 = w_3 = w_4$ and $w_5 = w_6 = w_7 = w_8$,

$$FoS_{toppling} = \left(\frac{12ab + 6ac}{3b^2 + 6bc + 2c^2} \right) \cdot \tan^{-1} \alpha \tag{A1.11}$$

So, the critical angle of toppling in Fig. A1.2a,

$$\alpha_{crit.} = \tan^{-1} \left(\frac{12ab + 6ac}{3b^2 + 6bc + 2c^2} \right) \tag{A1.12}$$

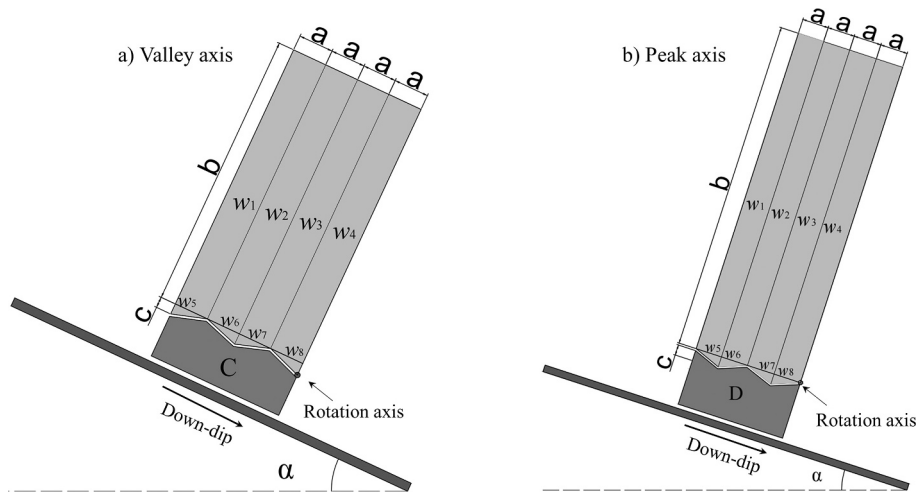


Fig. A1.2. a) Block C toppling with valley axis; b) block D toppling with peak axis.

A.1.3. Block D rotating around a peak axis

Fig. A1.2b shows the detail of block D with a regular rough base rotating around a peak pivot,

$$\begin{aligned} \sum M_{stabilizing} &= w_1 \cos \alpha \cdot \left(\frac{a}{2} + 3a \right) + w_2 \cos \alpha \cdot \left(\frac{a}{2} + 2a \right) + w_3 \cos \alpha \cdot \left(\frac{a}{2} + a \right) + \\ &+ w_4 \cos \alpha \cdot \frac{a}{2} + w_5 \cos \alpha \cdot \left(\frac{a}{3} + 3a \right) + w_6 \cos \alpha \cdot \left(\frac{2a}{3} + 2a \right) + \\ &+ w_7 \cos \alpha \cdot \left(\frac{a}{3} + a \right) + w_8 \cos \alpha \cdot \frac{2a}{3} + (w_5 + w_6 + w_7 + w_8) \sin \alpha \cdot \frac{c}{3} \end{aligned} \tag{A1.13}$$

$$\sum M_{overturning} = (w_1 + w_2 + w_3 + w_4) \sin \alpha \cdot \frac{b}{2} \tag{A1.14}$$

Accounting for the fact that $w_1 = w_2 = w_3 = w_4$ and $w_5 = w_6 = w_7 = w_8$, the equation of FoS can be simplified to,

$$FoS_{toppling} = \frac{c^2}{3b^2} + \left(\frac{4ab + 2ac}{b^2}\right) \cdot \tan^{-1} \alpha \tag{A1.15}$$

Then, the critical angle of toppling,

$$\alpha_{crit.} = \tan^{-1} \left(\frac{12ab + 6ac}{3b^2 - c^2}\right) \tag{A1.16}$$

A.1.4. Block F rotating around a valley axis

In the case of block F with the rotation axis in a valley as depicted in Fig. A1.3 a, we can obtain, the following formulae.

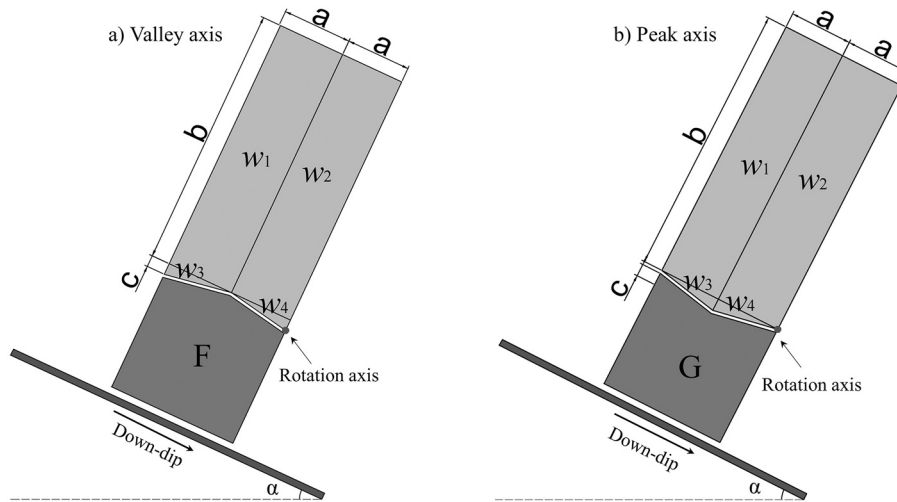


Fig. A1.3. a) Block F toppling with valley axis; b) Block G toppling with peak axis.

$$\sum M_{stabilizing} = w_1 \cos \alpha \cdot \left(\frac{a}{2} + a\right) + w_2 \cos \alpha \cdot \frac{a}{2} + w_3 \cos \alpha \cdot \left(\frac{2a}{3} + a\right) + w_4 \cos \alpha \cdot \frac{a}{3} \tag{A1.17}$$

$$\sum M_{overturning} = (w_1 + w_2) \sin \alpha \cdot \left(\frac{b}{2} + c\right) + (w_3 + w_4) \sin \alpha \cdot \frac{2c}{3} \tag{A1.18}$$

Based upon $w_1 = w_2$ and $w_3 = w_4$,

$$FoS_{toppling} = \left(\frac{6ab + 3ac}{3b^2 + 6bc + 2c^2}\right) \cdot \tan^{-1} \alpha \tag{A1.19}$$

Then, the critical toppling angle can be calculated,

$$\alpha_{crit.} = \tan^{-1} \left(\frac{6ab + 3ac}{3b^2 + 6bc + 2c^2}\right) \tag{A1.20}$$

A.1.5. Block G rotating around a peak axis

Block G illustrated in Fig. A1.3 b is symmetrical and rotated with a peak axis.

$$\sum M_{stabilizing} = w_1 \cos \alpha \cdot \left(\frac{a}{2} + a\right) + w_2 \cos \alpha \cdot \frac{a}{2} + w_3 \cos \alpha \cdot \left(\frac{a}{3} + a\right) + w_4 \cos \alpha \cdot \frac{2a}{3} + (w_3 + w_4) \cdot \sin \alpha \cdot \frac{c}{3} \tag{A1.21}$$

$$\sum M_{overturning} = (w_1 + w_2) \sin \alpha \cdot \frac{b}{2} \tag{A1.22}$$

$$FoS_{toppling} = \left(\frac{6ab + 3ac}{3b^2 - c^2}\right) \cdot \tan^{-1} \alpha \tag{A1.23}$$

The critical toppling angle can be obtained,

$$\alpha_{crit.} = \tan^{-1} \left(\frac{6ab + 3ac}{3b^2 - c^2}\right) \tag{A1.24}$$

Appendix B. Appendix

B.1. Individual equations for estimating the equivalent round corner radius for toppling of tested blocks (A, B, C, D, E-peak, and G)

Sometimes toppling is affected by the occurrence of irregularities in the corners. This effect can be analysed by considering that the corner of the rotation axis is rounded presenting a curvature radius, as analysed in section 2.2.2 for the simpler case. To account for this effect, in this Appendix B, we present the detailed individual calculations of factors of safety for the case of the blocks tested, in case they are considered to present round corners. Additionally, we include the computation of the equivalent curvature radius (r_c) as defined in section 4.1.1, for every block including peak and valley rotation axes, according to the particular critical angle physically observed ($\alpha_{phys.}$).

B.1.1. Block A, B and E-peak rotating with peak axis

Blocks A, B and E are asymmetrical with similar geometries; therefore, the failure mechanism of toppling can be computed for peak (Fig. A2.1a) and valley axes (Fig. A2.1b). As mentioned in physical tests, block E slid with the valley axis, so the equivalent curvature radius (r_c) was not considered. Additionally, an angle is needed for the calculations: δ_p ($= i$ effective roughness) which is the angle of roughness of the sub-triangle for toppling around a peak rotation axis or δ_v ($= 90-i$) the complementary angle of effective roughness for toppling around a valley axis.

For the case depicted in Fig. A2.1a,

$$\begin{aligned} \sum M_{stabilizing} = & w_1 \cos\alpha \cdot \left(2a + \frac{a}{2} - r \cos\delta_p\right) + w_2 \cos\alpha \cdot \left(a + \frac{a}{2} - r \cos\delta_p\right) + \\ & + w_3 \cos\alpha \cdot \left(\frac{a}{2} - r \cos\delta_p\right) + w_4 \cos\alpha \cdot \left(2a + \frac{2a}{3} - r \cos\delta_p\right) + \\ & + w_5 \cos\alpha \cdot \left(\frac{2a}{3} + \frac{2a}{3} - r \cos\delta_p\right) + w_6 \cos\alpha \cdot \left(\frac{2a}{3} - r \cos\delta_p\right) + \\ & + (w_4 + w_5 + w_6) \sin\alpha \cdot \left(\frac{c}{3} - r \sin\delta_p\right) \end{aligned} \tag{A2.1}$$

$$\sum M_{overturning} = (w_1 + w_2 + w_3) \sin\alpha \cdot \left(\frac{b}{2} + r \sin\delta_p\right) \tag{A2.2}$$

$$FoS_{toppling} = \left(\frac{27ab + 14ac - 9r \cos\delta_p \cdot (2b + c)}{9b^2 + 18br \sin\delta_p}\right) \cdot \tan^{-1}\alpha + \frac{c^2 - 3cr \sin\delta_p}{3b^2 + 6br \sin\delta_p} \tag{A2.3}$$

For limit equilibrium condition of physical test, where $FoS = 1$,

$$r = \frac{27ab + 14ac + (3c^2 - 9b^2) \tan\alpha_{phys.}}{(18b + 9c)(\tan\alpha_{phys.} \sin\delta_p + \cos\delta_p)} \tag{A2.4}$$

Then we can get the equivalent curvature radius (r_c),

$$r_c = r \cdot \tan\left(\frac{\delta_p + 90^\circ}{2}\right) \tag{A2.5}$$

$$r_c = \frac{27ab + 14ac + (3c^2 - 9b^2) \tan\alpha_{phys.}}{(18b + 9c)(\cos\delta_p + \sin\delta_p \tan\alpha_{phys.})} \cdot \tan\left(\frac{\delta_p + 90^\circ}{2}\right) \tag{A2.6}$$

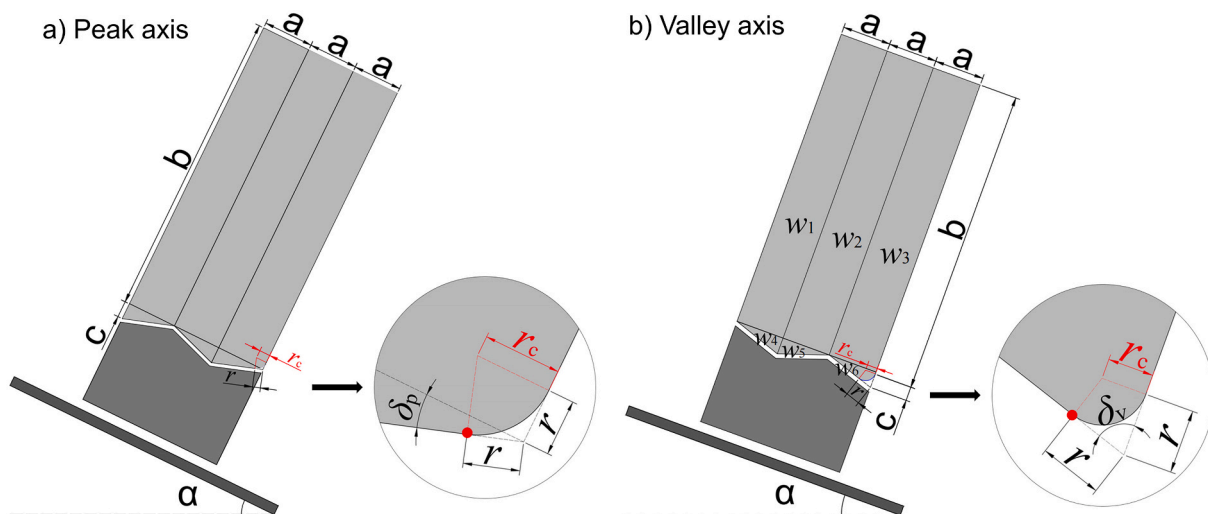


Fig. A2.1. a) Blocks A, B and E-peak toppling with peak axis; b) blocks A and B toppling with valley axis.

B.1.2. Block A and B rotating with valley axis

For the case of blocks A and B rotating with valley axis as shown in Fig. A2.1b,

$$\begin{aligned} \sum M_{stabilizing} = & w_1 \cos\alpha \cdot \left(2a + \frac{a}{2} - r \cdot \sin\delta_V\right) + w_2 \cos\alpha \cdot \left(a + \frac{a}{2} - r \cdot \sin\delta_V\right) \\ & + w_3 \cos\alpha \cdot \left(\frac{a}{2} - r \cdot \sin\delta_V\right) + w_4 \cos\alpha \cdot \left(\frac{a}{3} + a + \frac{a}{2} + \frac{a}{2} - r \cdot \sin\delta_V\right) + \\ & w_5 \cos\alpha \cdot \left(\frac{2a}{3} + \frac{a}{2} + \frac{a}{2} - r \cdot \sin\delta_V\right) + w_6 \cos\alpha \cdot \left(\frac{a}{3} - r \cdot \sin\delta_V\right) \end{aligned} \tag{A2.7}$$

$$\begin{aligned} \sum M_{overturning} = & (w_1 + w_2 + w_3) \sin\alpha \cdot \left(\frac{b}{2} + c - r \cdot \cos\delta_V\right) \\ & + (w_4 + w_5 + w_6) \sin\alpha \cdot \left(\frac{2c}{3} - r \cdot \cos\delta_V\right) \end{aligned} \tag{A2.8}$$

$$FoS_{toppling} = \tan^{-1}\alpha \cdot \frac{27ab + 13ac - 9r \sin\delta_V \cdot (2b + c)}{9b^2 + 6c^2 + 18bc - 9r \cos\delta_V \cdot (2b + c)} \tag{A2.9}$$

$$r = \frac{27ab + 13ac - (9b^2 + 6c^2 + 18bc) \tan\alpha_{phys.}}{(18b + 9c)(\sin\delta_V - \cos\delta_V \cdot \tan\alpha_{phys.})} \tag{A2.10}$$

$$r_c = \frac{27ab + 13ac - (9b^2 + 6c^2 + 18bc) \tan\alpha_{phys.}}{(18b + 9c)(\sin\delta_V - \cos\delta_V \cdot \tan\alpha_{phys.})} \cdot \tan \frac{\delta_V}{2} \tag{A2.11}$$

B.1.3. Block C rotating with valley axis

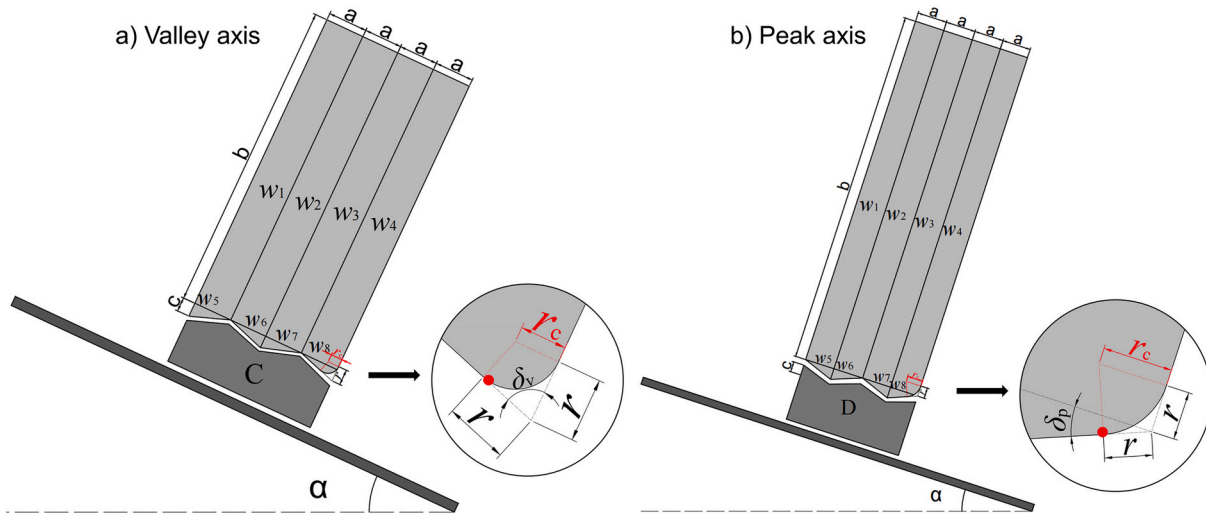


Fig. A2.2. a) Block C toppling with valley axis; b) Block D toppling with peak axis.

For the case of block C rotating with valley axis as shown in Fig. A2.2 a,

$$\begin{aligned} \sum M_{stabilizing} = & w_1 \cos\alpha \cdot \left[3a + \left(\frac{a}{2} - r \sin\delta_V\right)\right] + w_2 \cos\alpha \cdot \left[2a + \left(\frac{a}{2} - r \sin\delta_V\right)\right] \\ & + w_3 \cos\alpha \cdot \left[a + \left(\frac{a}{2} - r \sin\delta_V\right)\right] + w_4 \cos\alpha \cdot \left(\frac{a}{2} - r \sin\delta_V\right) + \\ & + w_5 \cos\alpha \cdot \left[\frac{2a}{3} + 2a + \frac{a}{2} + \left(\frac{a}{2} - r \sin\delta_V\right)\right] + \\ & + w_6 \cos\alpha \cdot \left[\frac{a}{3} + a + \frac{a}{2} + \left(\frac{a}{2} - r \sin\delta_V\right)\right] + \\ & + w_7 \cos\alpha \cdot \left[\frac{2a}{3} + \frac{a}{2} + \left(\frac{a}{2} - r \sin\delta_V\right)\right] + w_8 \cos\alpha \cdot \left(\frac{a}{3} - r \sin\delta_V\right) \end{aligned} \tag{A2.12}$$

$$\begin{aligned} \sum M_{overturning} = & (w_1 + w_2 + w_3 + w_4) \sin\alpha \cdot \left(\frac{b}{2} + c - r \cos\delta_V\right) \\ & + (w_5 + w_6 + w_7 + w_8) \sin\alpha \cdot \left(\frac{2c}{3} - r \cos\delta_V\right) \end{aligned} \tag{A2.13}$$

$$FoS_{toppling} = \frac{4ab + 2ac - r\sin\delta_V \cdot (2b + c)}{b^2 + \frac{2c^2}{3} + 2bc - r\cos\delta_V \cdot (2b + c)} \cdot \tan^{-1}\alpha \tag{A2.14}$$

$$r = \frac{4ab + 2ac - \tan\alpha_{phys} \cdot (b^2 + \frac{2}{3}c^2 + 2bc)}{(\sin\delta_V - \cos\delta_V \cdot \tan\alpha_{phys}) \cdot (2b + c)} \tag{A2.15}$$

$$r_c = \frac{4ab + 2ac - \tan\alpha_{phys} \cdot (b^2 + \frac{2}{3}c^2 + 2bc)}{(\sin\delta_V - \cos\delta_V \cdot \tan\alpha_{phys}) \cdot (2b + c)} \cdot \tan\frac{\delta_V}{2} \tag{A2.16}$$

B.1.4. Block D rotating with peak axis

For the case of block D rotating with valley axis as shown in Fig. A2.2 b,

$$\begin{aligned} \sum M_{stabilizing} = & w_1 \cos\alpha \cdot \left[3a + \left(\frac{a}{2} - r\cos\delta_P \right) \right] + \\ & + w_2 \cos\alpha \cdot \left[2a + \left(\frac{a}{2} - r\cos\delta_P \right) \right] + w_3 \cos\alpha \cdot \left[a + \left(\frac{a}{2} - r\cos\delta_P \right) \right] + \\ & + w_4 \cos\alpha \cdot \left(\frac{a}{2} - r\cos\delta_P \right) + w_5 \cos\alpha \cdot \left[\frac{a}{3} + 2a + \frac{a}{3} + \left(\frac{2a}{3} - r\cos\delta_P \right) \right] + \\ & + w_6 \cos\alpha \cdot \left[2a + \left(\frac{2a}{3} - r\cos\delta_P \right) \right] + w_7 \cos\alpha \cdot \left[\frac{a}{3} + \frac{a}{3} + \left(\frac{2a}{3} - r\cos\delta_P \right) \right] + \\ & + w_8 \cos\alpha \cdot \left(\frac{2a}{3} - r\cos\delta_P \right) + (w_5 + w_6 + w_7 + w_8) \sin\alpha \cdot \left(\frac{c}{3} - r\sin\delta_P \right) \end{aligned} \tag{A2.17}$$

$$\sum M_{overturning} = (w_1 + w_2 + w_3 + w_4) \sin\alpha \cdot \left(\frac{b}{2} + r\sin\delta_P \right) \tag{A2.18}$$

$$FoS_{toppling} = \tan^{-1}\alpha \cdot \frac{16ab + 8ac - 4r\cos\delta_P \cdot (2b + c)}{4b^2 + 8br\sin\delta_P} + \frac{c^2 - 3cr\sin\delta_P}{3b^2 + 6br\sin\delta_P} \tag{A2.19}$$

$$r = \frac{12ab + 6ac + (c^2 - 3b^2)\tan\alpha_{phys}}{(6b + 3c)(\cos\delta_P + \sin\delta_P \tan\alpha_{phys})} \tag{A2.20}$$

$$r_c = \frac{12ab + 6ac + (c^2 - 3b^2)\tan\alpha_{phys}}{(6b + 3c)(\cos\delta_P + \sin\delta_P \tan\alpha_{phys})} \cdot \tan\left(\frac{\delta_P + 90^\circ}{2}\right) \tag{A2.21}$$

B.1.5. Block G rotating with peak axis

For the case of block G rotating with valley axis as shown in Fig. A2.3,

$$\begin{aligned} \sum M_{stabilizing} = & w_1 \cos\alpha \cdot \left[a + \left(\frac{a}{2} - r\cos\delta_P \right) \right] + w_2 \cos\alpha \cdot \left(\frac{a}{2} - r\cos\delta_P \right) + \\ & + w_3 \cos\alpha \cdot \left[\frac{a}{3} + \frac{a}{3} + \left(\frac{2a}{3} - r\cos\delta_P \right) \right] + w_4 \cos\alpha \cdot \left(\frac{2a}{3} - r\cos\delta_P \right) + \\ & + (w_3 + w_4) \sin\alpha \cdot \left(\frac{c}{3} - r\sin\delta_P \right) \end{aligned} \tag{A2.22}$$

$$\sum M_{overturning} = (w_1 + w_2) \sin\alpha \cdot \left(\frac{b}{2} + r\sin\delta_P \right) \tag{A2.23}$$

$$FoS_{toppling} = \frac{c^2 - 3cr\sin\delta_P}{3b^2 + 6br\sin\delta_P} + \left[\frac{4ab + 4ac - 2r\cos\delta_P \cdot (2b + c)}{2b^2 + 4br\sin\delta_P} \right] \cdot \tan^{-1}\alpha \tag{A2.24}$$

$$r = \frac{6ab + 6ac + (c^2 - 3b^2)\tan\alpha_{phys}}{(6b + 3c)(\cos\delta_P + \sin\delta_P \tan\alpha_{phys})} \tag{A2.25}$$

$$r_c = \frac{6ab + 6ac + (c^2 - 3b^2)\tan\alpha_{phys}}{(6b + 3c)(\cos\delta_P + \sin\delta_P \tan\alpha_{phys})} \cdot \tan\left(\frac{\delta_P + 90^\circ}{2}\right) \tag{A2.26}$$

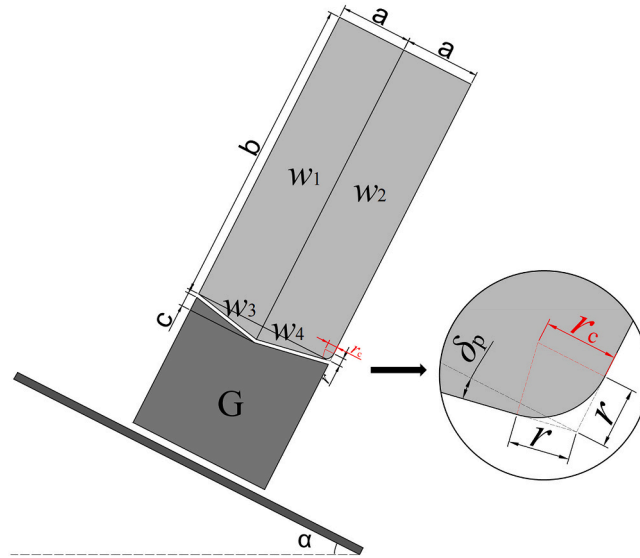


Fig. A2.3. Block G toppling with peak axis.

References

- Alzo'ubi, A.M., 2009. The Effect of Tensile Strength on the Stability of Rock Slopes (Ph.D. thesis). University of Alberta. <https://doi.org/10.7939/R32J68F7S>.
- Adhikary, D.P., Dyskin, A.V., 2007. Modelling of progressive and instantaneous failures of foliated rock slopes. *Rock Mech. Rock. Eng.* 40, 349–362. <https://doi.org/10.1007/s00603-006-0085-8>.
- Adhikary, D.P., Dyskin, A.V., Jewell, R.J., 1996. Numerical modelling of the flexural deformation of foliated rock slopes. *Int. J. Rock Mech. Min. Sci. Geomech. Abstr.* 33 [https://doi.org/10.1016/0148-9062\(96\)00008-3](https://doi.org/10.1016/0148-9062(96)00008-3), 595–6–6.
- Alejano, L.R., 2021. Considerations on failure mechanisms of rock slopes involving toppling. *IOP Conf. Ser. Earth Environ. Sci.* 833, 20–25 September, Turin, Italy. <http://iopscience.iop.org/article/10.1088/1755-1315/833/1/012004/meta>.
- Alejano, L.R., Alonso, E., 2005. Application of the shear and tensile strength reduction technique to obtain factors of safety of toppling and footwall rock slopes. In: *EUROCK 2005 Impact of Human Activity on the Geological Environment* (Brno, Czech Rep.), Balkema, Rotterdam.
- Alejano, L.R., Gómez-Márquez, I., Martínez-Alegría, R., 2010. Analysis of a complex toppling-circular slope failure. *Eng. Geol.* 114, 93–104. <https://doi.org/10.1016/j.enggeo.2010.03.005>.
- Alejano, L.R., Sánchez-Alonso, C., Pérez-Rey, I., Arzúa, J., Alonso, E., González, J., Beltramone, L., Ferrero, A.M., 2018a. Block toppling stability in the case of rock blocks with rounded edges. *Eng. Geol.* 234, 192–203. <https://doi.org/10.1016/j.enggeo.2018.01.010>.
- Alejano, L.R., Muralha, J., Ulusay, R., et al., 2018b. ISRM Suggested Method for Determining the Basic Friction Angle of Planar Rock Surfaces by Means of Tilt Tests. *Rock Mech. Rock Eng.* 51, 3853–3859. <https://doi.org/10.1007/s00603-018-1627-6>.
- Alejano, L.R., Veiga, M., Gómez-Márquez, I., Taboada, J., 2012. Stability of granite dry-stone masonry retaining walls: II. Relevant parameters and analytical and numerical studies of real walls. *Geotechnique* 62, 1027–1040. <https://doi.org/10.1680/geot.10.P.113>.
- Alejano, L.R., Carranza-Torres, C., Giani, G., Arzúa, J., 2015. Study of the stability against toppling of rock blocks with rounded edges based on analytical and experimental approaches. *Eng. Geol.* 195, 172–184. <https://doi.org/10.1016/j.enggeo.2015.05.030>.
- Alejano, L.R., Veiga, M., Pérez-Rey, I., Castro-Filgueira, U., Arzúa, J., Castro-Caicedo, Á. J., 2019. Analysis of a complex slope failure in a granodiorite quarry bench. *Bull. Eng. Geol. Environ.* 78, 1209–1224. <https://doi.org/10.1007/s10064-017-1160-y>.
- Amini, M., Ardestani, A., 2019. Stability analysis of the North-Eastern slope of Daralou copper open pit mine against a secondary toppling failure. *Eng. Geol.* 249, 89–101. <https://doi.org/10.1016/j.enggeo.2018.12.022>.
- Amini, M., Ardestani, A., Khosravi, M.H., 2017. Stability analysis of slide-toe-toppling failure. *Eng. Geol.* 228, 82–96. <https://doi.org/10.1016/j.enggeo.2017.07.008>.
- Ashby, J.P., 1971. *Sliding and Toppling Modes of Failure in Models and Jointed Rock Slopes* (MSc thesis). London University - Imperial College (London).
- Aydan, O., Kawamoto, T., 1992. The stability of slopes and underground openings against flexural toppling and their stabilization. *Rock Mech. Rock. Eng.* 25, 143–165. <https://doi.org/10.1007/BF01019709>.
- Barla, G., Borri-Brunetto, M., Devin, P., Zaninetti, A., 1995. Validation of a distinct element model for toppling rock slopes. In: *8th ISRM Congress*, pp. 417–421.
- Barton, N., 1973. Review of a new shear-strength criterion for rock joints. *Eng. Geol.* 7, 287–332. [https://doi.org/10.1016/0013-7952\(73\)90013-6](https://doi.org/10.1016/0013-7952(73)90013-6).
- Barton, N.R., 1981. *Shear Strength Investigation for Surface Mining*. Terra Tek, Inc., Salt Lake City, Utah.
- Barton, N., Choubey, V., 1977. The shear strength of rock joints in theory and practice. *Rock Mech.* 10, 1–54. <https://doi.org/10.1007/BF01261801>.
- Böhme, M., Hermanns, R.L., Oppikofer, T., Fischer, L., Bunkholt, H.S.S., Eiken, T., Pedrazzini, A., Derron, M.H., Jaboyedoff, M., Blikra, L.H., Nilsen, B., 2013. Analysing complex rock slope deformation at Stampa, western Norway, by integrating geomorphology, kinematics and numerical modelling. *Eng. Geol.* 154, 116–130. <https://doi.org/10.1016/j.enggeo.2012.11.016>.
- Brideau, M.A., Stead, D., 2010. Controls on block toppling using a three-dimensional distinct element approach. *Rock Mech. Rock. Eng.* 43, 241–260. <https://doi.org/10.1007/s00603-009-0052-2>.
- Cundall, P.A., 1971. A computer model for simulating progressive, large-scale movements in blocky rock systems. In: *Proceedings of the International Symposium on Rock Fracture*, 1. ISRM, Nancy, France. Paper II-8.
- Dawson, E.M., Roth, W.H., Drescher, A., 1999. Slope stability analysis by strength reduction. *Geotechnique* 49, 835–840. <https://doi.org/10.1680/geot.1999.49.6.835>.
- Goodman, R.E., Bray, J.W., 1976. Toppling of rock slopes in rock engineering for foundation and slopes. In: *Special Conference A.S.C.E.*, vol. 2. Boulder, Colorado, pp. 201–234.
- Gu, D.M., Huang, D., 2016. A complex rock topple-rock slide failure of an anacinal rock slope in the Wu Gorge, Yangtze River, China. *Eng. Geol.* 208, 165–180. <https://doi.org/10.1016/j.enggeo.2016.04.037>.
- Hoek, E., Bray, J., 1974. *Rock Slope Engineering*. Chapman & Hall.
- Ishida, T., 1990. Application of distinct element analysis to three simple block models aimed at practical application to toppling failure of fissured rock slopes. *Comput. Geotech.* 9, 341–353. [https://doi.org/10.1016/0266-352X\(90\)90046-X](https://doi.org/10.1016/0266-352X(90)90046-X).
- ISRM, 2007. The complete ISRM suggested methods for rock characterization, testing and monitoring: 1974–2006. In: Ulusay, R., Hudson, J.A. (Eds.), *Suggested Methods Prepared by the Commission on Testing Methods, International Society for Rock Mechanics*. Compilation Arranged by the ISRM Turkish National Group, Kozan Offset, Ankara, Turkey.
- ITASCA Cons. Group Inc, 2014. UDEC code - vers. 6.00. Minneapolis Minnesota, USA.
- ITASCA Cons. Group Inc, 2019. 3DEC Code - Vers. 5.20 Minneapolis Minnesota, USA.
- Lanaro, F., Jing, L., Stephansson, O., Barla, G., 1997. DEM modelling of laboratory tests of block toppling. *Int. J. Rock Mech. Min. Sci. Geomech. Abstr.* 34, 506–507. [https://doi.org/10.1016/S1365-1609\(97\)00116-0](https://doi.org/10.1016/S1365-1609(97)00116-0).
- Lemos, J.V., Costa, A.C., Bretas, E.M., 2011. Assessment of the seismic capacity of stone masonry walls with block models. *Comput. Meth. Appl. Sci.* 21, 221–235. https://doi.org/10.1007/978-94-007-0053-6_10.
- Martin, D.C., 1990. Deformation of open pit mine slopes by deep-seated toppling. *Int. J. Surf. Min. Reclam. Environ.* 4, 153–164. <https://doi.org/10.1080/09208119008944183>.
- Mendes, N., Zanotti, S., Lemos, J.V., 2020. Seismic performance of historical buildings based on discrete element method: an adobe church. *J. Earthq. Eng.* 24, 1270–1289. <https://doi.org/10.1080/13632469.2018.1463879>.
- Muniz-Menéndez, M., González-Gallego, J., Moreno-Robles, J., Pérez-Rey, I., Alejano, L.R., Riquelme, A., 2020. Stability analysis of balanced boulders: Methodology and case study. In: Li, C.C., Ødegaard, H., Macias, J. (Eds.), *ISRM International Symposium Eurock 2020—Hard Rock Engineering*. Trondheim, Norway, pp. 14–19.

- Muralha, J., 2002. Probabilistic analysis of toppling failure in rock slopes. In: *Rock Engineering for Mountainous Regions. Proceedings of the Regional Symposium of the ISRM. Eurock, Madeira, Portugal.*
- Myers, N.O., 1962. Characterization of surface roughness. *Wear* 5 (3), 182–189. [https://doi.org/10.1016/0043-1648\(62\)90002-9](https://doi.org/10.1016/0043-1648(62)90002-9).
- Patton, F.D., 1966. Multiple modes of shear failure in rock. In: *Proc. 1st Int. Congress on Rock Mech. Lisbon, 1*, pp. 509–513.
- Pérez-Rey, I., Alejano, L.R., Riquelme, A., González-deSantos, L., 2019. Failure mechanisms and stability analyses of granitic boulders focusing a case study in Galicia (Spain). *Int. J. Rock Mech. Min. Sci.* 119, 58–71. <https://doi.org/10.1016/j.ijrmms.2019.04.009>.
- Pérez-Rey, I., Muñiz-Menéndez, M., González, J., Vagnon, F., Walton, G., Alejano, L.R., 2021. Laboratory physical modelling of block toppling instability by means of tilt tests. *Eng. Geol.* 282 <https://doi.org/10.1016/j.enggeo.2021.105994>.
- Sagaseta, C., 1986. On the modes of instability of a rigid block on an inclined plane. *Rock Mech. Rock. Eng.* 19, 261–266. <https://doi.org/10.1007/BF01039998>.
- Sjöberg, J., 1999. Analysis of failure mechanisms in high rock slopes. In: Vouille, G., Berest, P. (Eds.), *9 Congrès International de Mécanique de Roches, Paris, France, vol. 1*. Balkema Publishers, A.A. / Taylor & Francis, The Netherlands, pp. 127–130.
- St John, C.M., 1972. *Numerical and Observational Methods of Determining the Behaviour of Rock Slopes in Opencast Mines*. University of London - Imperial College of Science and Technology.
- Stead, D., Wolters, A., 2015. A critical review of rock slope failure mechanisms: the importance of structural geology. *J. Struct. Geol.* 74, 1–23. <https://doi.org/10.1016/j.jsg.2015.02.002>.
- Stead, D., Eberhardt, E., Coggan, J.S., 2006. Developments in the characterization of complex rock slope deformation and failure using numerical modelling techniques. *Eng. Geol.* 83, 217–235. <https://doi.org/10.1016/j.enggeo.2005.06.033>.
- Tse, R., Cruden, D.M., 1979. Estimating joint roughness coefficients. *Int. J. Rock Mech. Min. Sci. Geomech. Abstr.* 16, 303–307. [https://doi.org/10.1016/0148-9062\(79\)90241-9](https://doi.org/10.1016/0148-9062(79)90241-9).
- Wyllie, D.C., Mah, C.W., 2004. *Rock Slope Engineering, Civil and Mining, fourth ed.* London and New York.
- Zhang, J.H., Chen, Z.Y., Wang, X.G., 2007. Centrifuge modelling of rock slopes susceptible to block toppling. *Rock Mech. Rock. Eng.* 40, 363–382. <https://doi.org/10.1007/s00603-006-0112-9>.
- Zheng, Y., Chen, C., Liu, T., Zhang, H., Sun, C., 2019. Theoretical and numerical study on the block-flexure toppling failure of rock slopes. *Eng. Geol.* 263, 105309 <https://doi.org/10.1016/j.enggeo.2019.105309>.